

Exploiting Target Location Distribution in MIMO Radar: PCRB vs. PSBP for Waveform Design

Lingyun Xu, *Graduate Student Member, IEEE*, Bowen Wang, *Graduate Student Member, IEEE*,
Huiyong Li and Ziyang Cheng, *Member, IEEE*

Abstract—This paper investigates the issue of how to exploit target location distribution for multiple input multiple output (MIMO) radar waveform design. We consider a MIMO radar aiming to estimate the unknown and random angular location parameters of a point target, whose distribution information can be exploited by the radar. First, we establish the models of the MIMO radar system and the target location distribution. Based on the considered models, we propose the first category of target location distribution exploitation methods by analyzing the radar direction-of-angle (DoA) estimation performance and deriving a general form of posterior Cramér-Rao bound (PCRB) as the lower bound of the mean square error of DoA estimation. Following this, to explore more insights, we proposed the second category of target location distribution exploitation methods by introducing a novel radar metric, probability scaled beampattern (PSBP), from the perspective of radar beampattern. To compare the two methods, we formulate the PCRB and PSBP oriented radar waveform design problems and propose corresponding low-complexity and convergence-guaranteed algorithms to tackle them. Finally, numerical simulations are conducted in different scenarios to provide a comprehensive evaluation and comparison of the radar performance.

Index Terms—MIMO radar, transmit waveform, posterior Cramér-Rao bound, DoA estimation.

I. INTRODUCTION

Multiple input multiple output (MIMO) radars employ multiple antennas at both transmitter and receiver, which can transmit multiple probing signals and receive multiple target echoes [1]–[4]. Compared with the traditional standard phase array radars, MIMO radars offer better accuracy of angular estimation and suppression of clutter/interference with a higher degree of freedom (DoF) [4], [5]. With these advantages, MIMO radars are promising in many applications, i.e., electronic reconnaissance [6], geophysical monitoring [7], medical imaging [8], etc. Driven by this, the investigations of MIMO radars have been widely carried out by many researchers so far.

Among the investigations of MIMO radars, the higher DoF provided by MIMO radar allows for flexible waveform design with proper properties, enhancing MIMO radar performance. Therefore, some works have focused on the MIMO radar waveform design with a desirable transmit beampattern [9]–[12]. For example, authors in [9] proposed a MIMO radar waveform design with the constant modulus constraint, where two methods were devised to minimize the square error and absolute error between the designed beampattern and the desired one, respectively. Another work in [11] proposed a

MIMO radar waveform design to achieve quasi-equiripple beampattern, where a new weighted l_p -norm matching metric was introduced and the matching error between the designed beampattern and the desired one was minimized. Moreover, the authors in [11] also extended the MIMO radar waveform design to the wideband in a spectrally dense environment in [12], where two design problems were formulated with different practical considerations by minimizing the beampattern matching error and peak sidelobe level (PSL), respectively. To realize a fairer control of both mainlobe and sidelobe levels, two methods for a constant modulus MIMO radar waveform design were proposed in [10], where the first one was to maximize the ratio of the minimum mainlobe level to the PSL, and the second one was to minimize the PSL subject to the mainlobe ripple constraint.

Compared with waveform design with the desirable transmit beampattern, some more quantifiable metrics, i.e., signal-to-interference-plus-noise ratio (SINR) [13]–[16], mutual information, relative entropy [17]–[19], etc., are also widely considered in MIMO radar design, which affects radar detection performance. For instance, authors in [13] considered a MIMO radar waveform design problem in the presence of interference, where the output SINR was maximized while meeting the constant modulus and similarity constraints. In [15], a spectrally compatible MIMO radar waveform design was proposed in the presence of multiple targets, where the waveform energy was minimized while satisfying the requirement of individual SINR for each target. Based on information theory, authors in [17] proposed the optimal MIMO radar waveform in colored noise, where two criteria were used: the mutual information between target impulse response and target echoes and the relative entropy between two hypotheses were maximized, respectively.

When focusing more intently on the problem of radar target localization in MIMO radar systems, a standard mathematical metric for measuring the accuracy of radar estimation of target parameters, Cramér-Rao bound (CRB) [20]–[22], is considered in MIMO radar design. In particular, the application of CRB is crucial in the estimation of direction-of-arrival (DoA) in MIMO radar systems. By calculating CRB, we can evaluate to what extent can the DoA estimation performance of different waveform design methods reach the theoretical lower bound [23]. For example, a CRB-based study for MIMO radar waveform optimization was carried out in [24], where the waveform design problem was formulated by minimizing the CRB of estimation for multiple targets in the presence of spatially colored interference and noises. Moreover, authors in [25] proposed a joint design of MIMO radar waveform and biased estimator in the presence of signal-dependent noises, where

L. Xu, B. Wang, H. Li and Z. Cheng are with the School of Information and Communication Engineering, University of Electronic Science and Technology of China, Chengdu 611731, China. (email: xusherly@std.uestc.edu.cn, bwwang@ieee.org, hlyli@uestc.edu.cn, zycheng@uestc.edu.cn).

a newly introduced constrained biased CRB was minimized to enhance the estimation performance. Another waveform design for MIMO radars to realize high-resolution localization was proposed in [26], where the asymptotic mean square error (MSE) of DoA estimation with multiple signal classification (MUSIC) algorithms was minimized to close to the CRB.

The aforementioned works [20]–[26] considered the time-invariant statistical models, where the location parameters of targets were assumed to be unknown and deterministic. However, in the time-varying systems, the location parameters of targets should be considered unknown and random, where the standard CRB is not applicable. In this case, a lower bound of random parameter estimation analogous to the CRB derived in [27], called posterior CRB (PCRB), also known as Bayesian CRB (BCRB), becomes a more appropriate metric [28], [29]. By using PCRB as a radar performance metric, the accuracy of estimation of random target parameters can be evaluated more properly, realizing more reliable target localization in practice. Since the prior information of distribution of target location parameters is essential for the derivation of PCRB, there have been many researches on the recursive inference of target location distribution information to utilize the PCRB to the radar sensing applications [30]–[35]. However, how to effectively exploit the inferred radar location distribution in the MIMO radar waveform design in order to optimize the radar estimation performance is still an open question and needs further investigation.

Motivated by the facts mentioned above, we investigate the problem of MIMO radar waveform designed by exploiting target location distribution. Specifically, the main contributions of this work can be summarized as follows.

- *Different target location distribution models:* Considering practical radar sensing scenarios, we establish two typical target angular location distribution models based on the statistical characteristics of the target location. Specifically, the first scenario is that the target is located on certain angular intervals with high occurrence probabilities, where the target location distribution is characterized by the uniform mixture model. The second scenario is that the target is located at certain angular points with high occurrence probabilities, where the target location distribution is characterized by the Gaussian mixture model.
- *PCRB oriented waveform optimization method:* Based on the considered system and target location distribution models, we analyze the MSE of DoA estimation and derive a general form of PCRB as the lower bound of the MSE, which is dependent on the target location distribution probability density function (PDF). Guided by this, we formulate a PCRB oriented waveform design problem, which can be solved by the proposed alternating direction method of multipliers (ADMM) based algorithm.
- *PSBP oriented waveform optimization method:* To provide more insights, we propose exploiting the target location distribution from the radar beam pattern perspective. Specifically, we introduce a novel metric, probability scaled beam pattern (PSBP), which is also dependent on the target location distribution PDF. For different

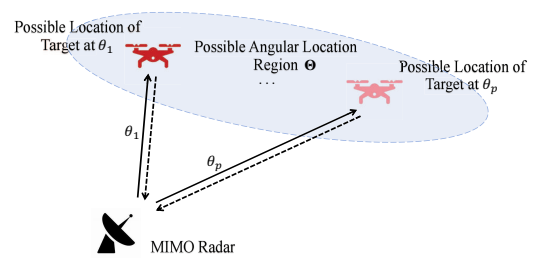


Fig. 1. Illustration of target localization with angular location distribution information available at the MIMO radar.

requirements of desirable beam pattern, we formulate two PSBP oriented waveform design problems: fair PSBP design and integrated PSBP design, which can be also solved by the proposed ADMM-based algorithms.

- *Multi-scenario radar sensing performance analysis:* We provide extensive numerical simulations in different scenarios to provide a comprehensive performance evaluation and comparison of the proposed waveform design methods.

Organization: Section II introduces the system model. Section III presents the target location distribution exploitation, gives the performance analysis, and formulates problems. Section IV and Section V derive the solutions to PCRB and PSBP oriented waveform design problems, respectively. Section VI demonstrates the numerical simulations and Section VII concludes this work.

Notations: This paper uses lower-case letters a for scalars, lower-case bold letters \mathbf{a} for vectors and upper-case bold letters \mathbf{A} for matrices. For a matrix \mathbf{A} , the element in the i -th row and the j -th column is denoted by $\mathbf{A}(i, j)$. \mathbb{C}^n and $\mathbb{C}^{m \times n}$ denote an n dimensional complex-valued vector and an m by n dimensional complex-valued space, respectively. $(\cdot)^T$ and $(\cdot)^H$ denote transpose and conjugate transpose operators, respectively. $|\cdot|$ represents a determinant or absolute value relying on the context. $\|\cdot\|_F$ and $\text{Tr}(\cdot)$ denote the Frobenius norm and trace, respectively. $\mathbb{E}\{\cdot\}$ denotes expectation. $\Re\{\cdot\}$ and $\Im\{\cdot\}$ denote the real part and imaginary part of a complex-valued number, respectively. $\mathcal{CN}(0, \mathbf{R})$ denotes the zero-mean complex Gaussian distribution with covariance matrix \mathbf{R} . $u(\cdot)$ and $\delta(\cdot)$ represent the unit step function and unit impulse function, respectively.

II. SYSTEM MODEL

A. Signal Model

As shown in Fig. 1, we consider a colocated MIMO radar, where the radar transmitter probes waveforms to illuminate targets, and the radar receiver collects the reflected echoes to conduct estimation. Unlike most existing papers [20]–[26], we assume that the exact angular location of the target is *unknown* and *random*, while its distribution is available at the radar and can be exploited. The colocated radar is equipped with M_t transmit antennas and M_r receive antennas, where the antenna arrays in both transmitter and receiver are assumed to be uniform linear arrays (ULAs) with half-wavelength element spacing d . The discrete-time waveform radiated by each antenna is represented by $\mathbf{x}_m(l)$, $m = 1, \dots, M_t, l = 1, \dots, L$, where L denotes the number of samples for each

radar pulse. Let $\mathbf{x}(l) = [\mathbf{x}_1(l), \dots, \mathbf{x}_{M_t}(l)]^T \in \mathbb{C}^{M_t}$ be the transmit waveform vector at the l -th sample of the M_t transmit antennas. Thus, the received signal at the l -th sample, $\mathbf{y}(l) \in \mathbb{C}^{M_r}$, can be expressed as

$$\mathbf{y}(l) = \varsigma \mathbf{a}_r(\theta) \mathbf{a}_t^H(\theta) \mathbf{x}(l) + \mathbf{z}(l), \quad (1)$$

where ς denotes the complex amplitude of the target, which is assumed to be an unknown and deterministic parameter, $\mathbf{z}(l) \sim \mathcal{CN}(0, \sigma_r^2 \mathbf{I}_{M_r})$ denotes the additive white Gaussian noise (AWGN). The transmit and receive steering vectors are respectively given by

$$\mathbf{a}_t(\theta) = \left[e^{-j\pi \frac{M_t-1}{2} d \sin \theta}, \dots, e^{j\pi \frac{M_t-1}{2} d \sin \theta} \right]^T \in \mathbb{C}^{M_t},$$

$$\mathbf{a}_r(\theta) = \left[e^{-j\pi \frac{M_r-1}{2} d \sin \theta}, \dots, e^{j\pi \frac{M_r-1}{2} d \sin \theta} \right]^T \in \mathbb{C}^{M_r}.$$

By collecting L samples of the received signal, the received signal during one frame, $\mathbf{Y} \in \mathbb{C}^{M_r \times L}$, can be given by

$$\mathbf{Y} = [\mathbf{y}(1), \dots, \mathbf{y}(L)] = \varsigma \mathbf{A}(\theta) \mathbf{X} + \mathbf{Z}, \quad (2)$$

where $\mathbf{X} = [\mathbf{x}(1), \dots, \mathbf{x}(L)] \in \mathbb{C}^{M_t \times L}$ is the space-time transmit waveform matrix, and we define $\mathbf{A}(\theta) = \mathbf{a}_r(\theta) \mathbf{a}_t^H(\theta)$ and $\mathbf{Z} = [\mathbf{z}(1), \dots, \mathbf{z}(L)]$.

The radar transmitter typically exhibits a large dynamic range. To avoid out-of-band radiation and signal distortion, the peak-to-average-power ratio (PAPR) of the radar transmit waveforms should be properly limited [36]–[38]. To this end, we define the PAPR as follows

$$\text{PAPR}(\mathbf{X}) = \frac{\max_{m,l} |\mathbf{X}(m,l)|^2}{\frac{1}{M_t L} \|\mathbf{X}\|_F^2} \leq \kappa, \forall m, l, \quad (3)$$

where $\kappa \geq 1$ denotes the PAPR threshold of the radar system. Without loss of generality, we assume that the total transmit power is P , i.e., $\|\mathbf{X}\|_F^2 = P$. By substituting the transmit power budget to (3), we can rewrite the PAPR constraint into

$$\text{PAPR}(\mathbf{X}) \rightarrow \begin{cases} \|\mathbf{X}\|_F^2 = P, \\ \frac{M_t L}{P} \max_{m,l} |\mathbf{X}(m,l)|^2 \leq \kappa, \forall m, l. \end{cases} \quad (4)$$

B. Target Location Distribution Model

As shown in Fig. 1, a MIMO radar aims at estimating the DoA of a point target. It is assumed that the exact angle $\theta \in \Theta = [-\pi/2, \pi/2]$ of the target is an *unknown* and *random* parameter, whose location distribution information inferred from historical observations and empirical data is available at the radar [30]–[35]. Let $f(\theta_p)$ denote the target angular location PDF at θ_p . In the following, based on the statistical characteristics of the angular location θ and the considered practical scenarios, we proceed with modeling the continuous PDF of θ as $f(\theta)$, which leads to the following two categories.

1) *Distribution Model 1: High Occurrence Probability on Certain Angular Intervals.* Suppose the target angular location distribution available at the radar is that the potential target may be located on K angular intervals, $\Theta_1, \dots, \Theta_K$.

We assume that the probability of the target appearing on the k -th possible angular location interval is p_k and $\sum_{k=1}^K p_k =$

1, where the target angle obeys uniform distribution on each possible angular location interval. The continuous PDF of the k -th possible angular location interval is then given by

$$f_k(\theta) = p_k \frac{1}{\theta_{k2} - \theta_{k1}}, \theta \in \Theta_k, \quad (5)$$

where θ_{k1} and θ_{k2} denote the left and right end points of the k -th possible angular location interval Θ_k , respectively.

Based on this model, we can characterize the target angular location distribution by defining the continuous mixture uniform PDF as

$$f(\theta) = \sum_{k=1}^K p_k \frac{1}{\theta_{k2} - \theta_{k1}} [u(\theta - \theta_{k1}) - u(\theta - \theta_{k2})], \quad (6)$$

which is the sum of the probability-weighted K PDFs of the uniform distribution on possible target angular location distribution intervals.

2) *Distribution Model 2: High Occurrence Probability at Certain Angular Points.* Then, we consider another scenario, where the target location distribution information available at the radar is that the potential target may be located at K angular points, $\theta_1, \dots, \theta_K$, with a small uncertainty. We assume that the probability of the target appearing around the k -th point is p_k and $\sum_{k=1}^K p_k = 1$. The continuous PDF around the k -th possible point is modeled as

$$f_k(\theta) = \frac{1}{\sqrt{2\pi}\sigma_\theta} \exp\left\{-\frac{(\theta - \theta_k)^2}{2\sigma_\theta^2}\right\}, \quad (7)$$

where θ_k and σ_θ^2 respectively denote the mean and the small variance of the k -th Gaussian PDF. Then, we can model the distribution model of the target angle as a mixture Gaussian PDF, which is given by

$$f(\theta) = \sum_{k=1}^K p_k f_k(\theta). \quad (8)$$

In this paper, we aim to discuss how to properly use the target location distribution information to design radar waveforms that improve radar estimation performance. Thus, in the following sections, we will discuss the exploitation of target location distribution from the perspectives of the PCRB and beam pattern design.

III. TARGET LOCATION DISTRIBUTION EXPLOITATION AND PERFORMANCE ANALYSIS

In this section, we analyze radar DoA estimation performance using the MSE estimator, yielding a novel PCRB-based target location distribution exploitation method. Then, we propose exploiting target location distribution from the beam pattern perspective and derive a novel PSBP metric.

A. PCRB-based Target Location Distribution Exploitation

Since we focus on radar estimation, it is straightforward to evaluate the estimation performance from the PCRB perspective [28], [29]. Given that we assume the target location distribution is available, we will focus on the PCRB analysis [28], [29]. Because we consider a general $f(\theta)$ with two

typical distribution models, in the following sections, we will formulate the general form of PCRB of the considered radar system and apply the general results to these two typical cases.

1) *General Form of PCRB*: For notations, we can define the collection of the target's unknown and random parameter as $\boldsymbol{\omega} = [\theta, \varsigma_R, \varsigma_I]^T$, where $\varsigma_R = \Re\{\varsigma\}$ and $\varsigma_I = \Im\{\varsigma\}$. It is assumed that θ and ς are independent of each other.

We suppose that $\hat{\boldsymbol{\omega}}$ is the unbiased estimation of $\boldsymbol{\omega}$ and then the estimation MSE of $\boldsymbol{\omega}$ is $\text{MSE}_{\boldsymbol{\omega}}(\hat{\boldsymbol{\omega}}) = \mathbb{E}\{\|\boldsymbol{\omega} - \hat{\boldsymbol{\omega}}\|_F^2\}$. Since the MSE is equal to the generalized error variance for unbiased estimator [39] and the information of $\boldsymbol{\omega}$ can be exploited, we define PCRB as the lower bound of the MSE

$$\text{MSE}_{\boldsymbol{\omega}}(\hat{\boldsymbol{\omega}}) \geq \text{PCRB}_{\boldsymbol{\omega}|\mathbf{Y}} = \left| \mathbf{F}_{\boldsymbol{\omega}|\mathbf{Y}}^{-1} \right|, \quad (9)$$

where $\mathbf{F}_{\boldsymbol{\omega}|\mathbf{Y}} \in \mathbb{C}^{3 \times 3}$ denotes the posterior FIM for the estimation of $\boldsymbol{\omega}$, which is given by

$$\mathbf{F}_{\boldsymbol{\omega}|\mathbf{Y}} = \mathbf{F}_S + \mathbf{F}_P, \quad (10)$$

where \mathbf{F}_S denotes the FIM extracted from the received signal, and \mathbf{F}_P denotes the FIM extracted from the distribution information. Specifically, \mathbf{F}_S and \mathbf{F}_P are expressed as

$$\mathbf{F}_S = \mathbb{E} \left\{ \frac{\partial \ln(f(\mathbf{Y}|\boldsymbol{\omega}))}{\partial \boldsymbol{\omega}} \left(\frac{\partial \ln(f(\mathbf{Y}|\boldsymbol{\omega}))}{\partial \boldsymbol{\omega}} \right)^H \right\}, \quad (11a)$$

$$\mathbf{F}_P = \mathbb{E} \left\{ \frac{\partial \ln f(\boldsymbol{\omega})}{\partial \boldsymbol{\omega}} \left(\frac{\partial \ln f(\boldsymbol{\omega})}{\partial \boldsymbol{\omega}} \right)^H \right\}, \quad (11b)$$

where $f(\mathbf{Y}|\boldsymbol{\omega})$ denotes the conditional PDF of \mathbf{Y} with a given $\boldsymbol{\omega}$ and $f(\boldsymbol{\omega})$ denotes the PDF of $\boldsymbol{\omega}$. Accordingly, we can divide the derivation of the posterior FIM (10) into two steps, the derivation of \mathbf{F}_S and the derivation of \mathbf{F}_P .

Step 1: The Derivation of \mathbf{F}_S . We deal with the FIM extracted from the received signal, \mathbf{F}_S , as follows. The joint conditional distribution of $\mathbf{Y} = [\mathbf{y}(1), \dots, \mathbf{y}(L)]$ is given by

$$f(\mathbf{Y}|\boldsymbol{\omega}) = \frac{1}{\pi^{M_r L} |\sigma_r^2 \mathbf{I}_{M_r L}|} \exp \left\{ -\frac{\|\mathbf{Y} - \varsigma \mathbf{A}(\theta) \mathbf{X}\|_F^2}{\sigma_r^2} \right\}. \quad (12)$$

Accordingly, the log-likelihood function of \mathbf{Y} given $\boldsymbol{\omega}$ can be calculated as

$$\begin{aligned} l(\mathbf{Y}|\boldsymbol{\omega}) &= \ln f(\mathbf{Y}|\boldsymbol{\omega}) \\ &= -M_r L \ln(\pi \sigma_r^2) - \frac{\|\mathbf{Y}\|_F^2}{\sigma_r^2} - \frac{|\varsigma|^2 \|\mathbf{A}(\theta) \mathbf{X}\|_F^2}{\sigma_r^2} \\ &\quad + \frac{2\Re\{\text{Tr}\{\varsigma^* \mathbf{X}^H \mathbf{A}^H(\theta) \mathbf{Y}\}\}}{\sigma_r^2}. \end{aligned} \quad (13)$$

Then, we have the following proposition to calculate \mathbf{F}_S .

Proposition 1: Based on (11a) and (13), \mathbf{F}_S can be decomposed into blocks, which is given by

$$\mathbf{F}_S = \begin{bmatrix} F_{\theta\theta} & \mathbf{F}_{\theta\varsigma} \\ \mathbf{F}_{\varsigma\theta} & \mathbf{F}_{\varsigma\varsigma} \end{bmatrix} \in \mathbb{C}^{3 \times 3}, \quad (14)$$

where

$$F_{\theta\theta} = \frac{2|\varsigma|^2}{\sigma_r^2} \text{Tr}\{\mathbf{X}^H \boldsymbol{\Xi}_1 \mathbf{X}\}, \quad (15a)$$

$$\mathbf{F}_{\theta\varsigma} = \frac{2}{\sigma_r^2} \text{Tr}\{\mathbf{X}^H \boldsymbol{\Xi}_2 \mathbf{X}\} [\varsigma_R, \varsigma_I], \quad (15b)$$

$$\mathbf{F}_{\varsigma\theta} = \mathbf{F}_{\theta\varsigma}^H = \left(\frac{2}{\sigma_r^2} \text{Tr}\{\mathbf{X}^H \boldsymbol{\Xi}_2 \mathbf{X}\} [\varsigma_R, \varsigma_I] \right)^H, \quad (15c)$$

$$\mathbf{F}_{\varsigma\varsigma} = \frac{2}{\sigma_r^2} \text{Tr}\{\mathbf{X}^H \boldsymbol{\Xi}_3 \mathbf{X}\} \mathbf{I}_2, \quad (15d)$$

with

$$\begin{aligned} \boldsymbol{\Xi}_1 &= \int_{-\pi/2}^{\pi/2} f(\theta) \|\dot{\mathbf{a}}_r(\theta)\|_F^2 \mathbf{a}_t(\theta) \mathbf{a}_t^H(\theta) d\theta \\ &\quad + M_r \int_{-\pi/2}^{\pi/2} f(\theta) \dot{\mathbf{a}}_t(\theta) \dot{\mathbf{a}}_t^H(\theta) d\theta, \end{aligned} \quad (16a)$$

$$\boldsymbol{\Xi}_2 = M_r \int_{-\pi/2}^{\pi/2} f(\theta) \dot{\mathbf{a}}_t(\theta) \mathbf{a}_t^H(\theta) d\theta, \quad (16b)$$

$$\boldsymbol{\Xi}_3 = M_r \int_{-\pi/2}^{\pi/2} f(\theta) \mathbf{a}_t(\theta) \mathbf{a}_t^H(\theta) d\theta, \quad (16c)$$

$\dot{\mathbf{a}}(\theta)$ denoting the derivative of $\mathbf{a}(\theta)$ about θ .

Proof: Please refer to supplementary material (SM) Appendix A. ■

Step 2: The Derivation of \mathbf{F}_P . We calculate the FIM extracted from the distribution, \mathbf{F}_P . Since the angle θ is an unknown and random parameter, and complex amplitude ς is an unknown and deterministic parameter, we can derive

$$\frac{\partial \ln f(\boldsymbol{\omega})}{\partial \boldsymbol{\omega}} = \left[\frac{\partial \ln f(\theta)}{\partial \theta}, 0, 0 \right]^T. \quad (17)$$

Based on (11b) and (17), \mathbf{F}_P can be calculated and decomposed into

$$\mathbf{F}_P = \begin{bmatrix} B_{\theta\theta} & 0 & 0 \\ 0 & 0 & 0 \\ 0 & 0 & 0 \end{bmatrix} \in \mathbb{C}^{3 \times 3}, \quad (18)$$

where

$$B_{\theta\theta} = \int_{-\pi/2}^{\pi/2} f(\theta) \left(\frac{\partial \ln f(\theta)}{\partial \theta} \right)^2 d\theta \triangleq \Lambda \quad (19)$$

Based on the above two-step formulations, the PCRB in (9) can be expressed as

$$\text{PCRB}_{\boldsymbol{\omega}|\mathbf{Y}} = \left[\begin{bmatrix} F_{\theta\theta} + B_{\theta\theta} & \mathbf{F}_{\theta\varsigma} \\ \mathbf{F}_{\varsigma\theta} & \mathbf{F}_{\varsigma\varsigma} \end{bmatrix}^{-1} \right]. \quad (20)$$

To characterize the DoA estimation performance of the MIMO radar, we derive the PCRB for the estimation of θ with unknown ς , $\text{PCRB}_{\theta}(\mathbf{X})$, by extracting the upper-left block corresponding to θ [40], which is given by

$$\begin{aligned} \text{PCRB}_{\theta}(\mathbf{X}) &= [F_{\theta\theta} + B_{\theta\theta} - \mathbf{F}_{\theta\varsigma} \mathbf{F}_{\varsigma\varsigma}^{-1} \mathbf{F}_{\varsigma\theta}]^{-1} \\ &= \left[\frac{2|\varsigma|^2}{\sigma_r^2} \text{Tr}\{\mathbf{X}^H \boldsymbol{\Xi}_1 \mathbf{X}\} - \frac{2|\varsigma|^2}{\sigma_r^2} \frac{|\text{Tr}\{\mathbf{X}^H \boldsymbol{\Xi}_2 \mathbf{X}\}|^2}{\text{Tr}\{\mathbf{X}^H \boldsymbol{\Xi}_3 \mathbf{X}\}} + \Lambda \right]^{-1}. \end{aligned} \quad (21)$$

2) *PCRB for Typical Distribution Model*: Note that $\text{PCRB}_\theta(\mathbf{X})$ is related to Ξ_1, Ξ_2, Ξ_3 , and Λ , which are determined by the distribution model. Therefore, in the following, we will calculate Λ under the two considered distribution models mentioned in Sec. II-B¹.

Distribution Model 1: Applying the mixture uniform PDF of distribution model 1 in (6) to Λ in (19), we have ²

$$\Lambda = \int_{-\infty}^{\infty} \frac{\sum_{k=1}^K \left(p_k \frac{1}{\theta_{k2} - \theta_{k1}} \right)^2 [\delta(\theta - \theta_{k1}) - \delta(\theta - \theta_{k2})]}{\sum_{k=1}^K p_k \frac{1}{\theta_{k2} - \theta_{k1}} [u(\theta - \theta_{k1}) - u(\theta - \theta_{k2})]} d\theta \triangleq C_1.$$

Submitting $\Xi_1, \Xi_2, \Xi_3, \Lambda$ into $\text{PCRB}_\theta(\mathbf{X})$ (21), we obtain the PCRB for distribution model 1.

Distribution Model 2: Applying the mixture Gaussian PDF of distribution model 2 in (8) to Λ in (19), we have

$$\Lambda = \frac{1}{\sigma_\theta^2} \int_{-\infty}^{\infty} \frac{\sum_{k_1=1}^K \sum_{k_2=1}^K p_{k_1} p_{k_2} f_{k_1}(\theta) f_{k_2}(\theta) \left(\frac{\theta_{k_2} - \theta_{k_1}}{\sigma_\theta^2} \right)^2}{2 \sum_{k=1}^K p_k f_k(\theta)} d\theta \triangleq C_2.$$

Submitting $\Xi_1, \Xi_2, \Xi_3, \Lambda$ into $\text{PCRB}_\theta(\mathbf{X})$ (21), we obtain the PCRB for distribution model 2.

3) *Problem Formulation*: Based on the above PCRB-based target location distribution exploitation, we aim to design the radar transmit waveform to minimize the PCRB, thereby improving the radar DoA estimation performance. Specifically, the PCRB oriented waveform design problem is formulated by minimizing the PCRB subject to the PAPR and transmit power constraints, which is given by

$$\mathcal{P}_{\text{PCRB}, \mathbf{X}}^{1-1} \begin{cases} \min_{\mathbf{X}} \text{PCRB}_\theta(\mathbf{X}) & (22a) \\ \text{s.t. } \|\mathbf{X}\|_F^2 = P & (22b) \\ \frac{M_t L}{P} \max_{m,l} |\mathbf{X}(m,l)|^2 \leq \kappa, \forall m,l, & (22c) \end{cases}$$

where κ represents the PAPR requirement.

Before proceeding, we make the following remarks.

Remark 1 (Is minimizing PCRB effective?): It is worth mentioning that the derived PCRB (21) is just a theoretical lower bound for MSE of estimation of the target angular location θ . Although the problem (22) is to minimize the PCRB, whether a lower bound can be reached in practice depends on various factors. This raises a critical question: “Is minimizing the PCRB effective?” Or “Is there any other method to effectively exploit target location distribution?”

B. PSBP-based Target Location Distribution Exploitation

It is widely acknowledged that transmit beampattern should be focused on the potential direction of the target to enhance radar detection and estimation performance. This idea motivates us to address *Remark 1* from the beampattern design perspective and explore another way to exploit target location distribution in the following.

¹The calculations of Ξ_1, Ξ_2, Ξ_3 are based on (16a)-(16c), which are straightforward and thus omitted here.

²Since the probability of the target appearing outside Θ can be considered zero, it is rational to approximately transform the integral interval from $[-\pi/2, \pi/2]$ to $[-\infty, \infty]$ for convenience of calculation.

1) *PSBP Metric*: The radar transmit power towards angle θ is defined as $\mathcal{E}(\theta) = \|\mathbf{a}_t^H(\theta_p)\mathbf{X}\|_F^2$. Note that $\mathcal{E}(\theta) = \|\mathbf{a}_t^H(\theta)\mathbf{X}\|_F^2$ is highly dependent on θ without exploiting the target location distribution. Therefore, a novel radar beampattern metric, called PSBP, is proposed to characterize the radar transmit power towards θ_p scaled by the PDF $f(\theta_p)$. Specifically, the PSBP at the p -th point in the possible target angular location region is defined as

$$\text{PSBP}_{\theta_p}^w(\mathbf{X}) = w(f(\theta_p)) \|\mathbf{a}_t^H(\theta_p)\mathbf{X}\|_F^2, \theta_p \in \Theta, \quad (23)$$

where $w(f(\theta_p))$ denotes the scaling weight function of the angular location PDF $f(\theta_p)$ at angle θ_p . The specific form of $w(f(\theta_p))$ is determined by the requirements of waveform optimization.

2) *Problem Formulation*: Based on the newly proposed PSBP, we present the following two PSBP oriented waveform problems for different design requirements.

Fair PSBP Design. Based on the target location distribution model, the target of interest occurs at different possible locations with different probabilities. To ensure the beampattern is fair towards all possible locations, we propose a fair PSBP design problem, where the minimal PSBP is maximized. Therefore, the design problem can be formulated as follows

$$\mathcal{P}_{\text{PSBP}, \mathbf{X}}^{2-1} \begin{cases} \max_{\mathbf{X}} \min_{\theta_p \in \Theta} \text{PSBP}_{\theta_p}^w(\mathbf{X}) & (24a) \\ \text{s.t. } \|\mathbf{X}\|_F^2 = P & (24b) \\ \frac{M_t L}{P} \max_{m,l} |\mathbf{X}(m,l)|^2 \leq \kappa, \forall m,l, & (24c) \end{cases}$$

where the scaling weight function is selected as $w(f(\theta_p)) = \frac{1}{f(\theta_p)}$, leading to $\text{PSBP}_{\theta_p}^w(\mathbf{X}) = \frac{1}{f(\theta_p)} \|\mathbf{a}_t^H(\theta_p)\mathbf{X}\|_F^2$.

Integrated PSBP Design. In addition to maintaining fairness towards all possible locations, it is straightforward to transmit more power towards directions with higher probabilities. Thus, we propose an integrated PSBP design problem, where the integrated PSBP is maximized. Therefore, the design problem can be formulated as follows:

$$\mathcal{P}_{\text{PSBP}, \mathbf{X}}^{3-1} \begin{cases} \max_{\mathbf{X}} \sum_{\theta_p \in \Theta} \text{PSBP}_{\theta_p}^w(\mathbf{X}) & (25a) \\ \text{s.t. } \|\mathbf{X}\|_F^2 = P & (25b) \\ \frac{M_t L}{P} \max_{m,l} |\mathbf{X}(m,l)|^2 \leq \kappa, \forall m,l, & (25c) \end{cases}$$

where the scaling weight function is selected as $w(f(\theta_p)) = f(\theta_p)$, leading to $\text{PSBP}_{\theta_p}^w(\mathbf{X}) = f(\theta_p) \|\mathbf{a}_t^H(\theta_p)\mathbf{X}\|_F^2$.

Before moving to solutions to design problems, we make the following remark.

Remark 2 (Comparison between PCRB and PSBP Metrics): *i)* Compared with PSBP, PCRB has a more specific meaning, denoting the lower bound of radar estimation performance. However, although many studies show that designing radar transmit beampattern with proper direction can improve radar estimation performance, the mathematical relationship between the PSBP and estimation performance is still unclear. *ii)* PCRB requires pre-calculating many distribution parameters, $\Xi_1, \Xi_2, \Xi_3, \Lambda$, leading to higher computational complexity. In contrast, the newly proposed PSBP is more compact and explicit, without the need for pre-calculations.

IV. SOLUTION TO PCRB ORIENTED WAVEFORM DESIGN

In this section, we first simplify the PCRB oriented waveform design problem, then derive a solution, and finally conclude with a summary of the proposed method.

A. Problem Reformulation

1) *Step 1: Simplification to $\text{PCRB}_\theta(\mathbf{X})$.* Since the objective function $\text{PCRB}_\theta(\mathbf{X})$ in (22) is a complicated fractional function with the inverse operation, we present the following proposition to simplify it into a more tractable form.

Proposition 2: We introduce an upper bound of PCRB, $\overline{\text{PCRB}}_\theta(\mathbf{X})$ as

$$\text{PCRB}_\theta(\mathbf{X}) < \left[\Lambda + \frac{2|\zeta|^2}{\sigma_r^2} \text{Tr} \{ \mathbf{X}^H \boldsymbol{\Xi}_0 \mathbf{X} \} \right]^{-1} \triangleq \overline{\text{PCRB}}_\theta(\mathbf{X}), \quad (26)$$

where $\boldsymbol{\Xi}_0 = \int_{-\pi/2}^{\pi/2} f(\theta) \|\dot{\mathbf{a}}_r(\theta)\|_F^2 \mathbf{a}_t(\theta) \mathbf{a}_t^H(\theta) d\theta$.

Proof: Please refer to SM Appendix B. ■

According to *Proposition 2* and noting that Λ is irrelevant to \mathbf{X} , the $\mathcal{P}_{\text{PCRB},\mathbf{X}}^{1-1}$ can be simplified as

$$\mathcal{P}_{\text{PCRB},\mathbf{X}}^{1-2} \begin{cases} \min_{\mathbf{X}} & -\text{Tr} \{ \mathbf{X}^H \boldsymbol{\Xi}_0 \mathbf{X} \} \\ \text{s.t.} & \|\mathbf{X}\|_F^2 = P \\ & |\mathbf{X}(m,l)|^2 \leq \frac{\kappa P}{M_t L}, \forall m,l. \end{cases} \quad (27a)$$

$$\text{s.t.} \quad \|\mathbf{X}\|_F^2 = P \quad (27b)$$

$$|\mathbf{X}(m,l)|^2 \leq \frac{\kappa P}{M_t L}, \forall m,l. \quad (27c)$$

2) *Step 2: Application of ADMM Framework to $\mathcal{P}_{\text{PCRB},\mathbf{X}}^{1-2}$.* To derive an efficient solution to $\mathcal{P}_{\text{PCRB},\mathbf{X}}^{1-2}$, we propose introducing an auxiliary variable \mathbf{U} to decouple the objective and constraints, leading to the following problem.

$$\mathcal{P}_{\text{PCRB},\mathbf{X}}^{1-3} \begin{cases} \min_{\mathbf{X},\mathbf{U}} & -\text{Tr} \{ \mathbf{X}^H \boldsymbol{\Xi}_0 \mathbf{X} \} \\ \text{s.t.} & \|\mathbf{X}\|_F^2 = P \\ & |\mathbf{U}(m,l)|^2 \leq \frac{\kappa P}{M_t L}, \forall m,l \\ & \mathbf{X} = \mathbf{U}. \end{cases} \quad (28a)$$

$$\text{s.t.} \quad \|\mathbf{X}\|_F^2 = P \quad (28b)$$

$$|\mathbf{U}(m,l)|^2 \leq \frac{\kappa P}{M_t L}, \forall m,l \quad (28c)$$

$$\mathbf{X} = \mathbf{U}. \quad (28d)$$

By penalizing the equality constraint (28d) into the objective function, we equivalently rewrite the problem (28) into an augmented Lagrangian (AL) minimization problem as follows

$$\mathcal{P}_{\text{PCRB},\mathbf{X}}^{1-4} \begin{cases} \min_{\mathbf{X},\mathbf{U},\mathbf{D}_1} & \mathcal{L}_1(\mathbf{X}, \mathbf{U}, \mathbf{D}_1) \\ \text{s.t.} & (28b) \text{ and } (28c), \end{cases} \quad (29a)$$

$$\text{s.t.} \quad (28b) \text{ and } (28c), \quad (29b)$$

The associated AL function is given by

$$\mathcal{L}_1(\mathbf{X}, \mathbf{U}, \mathbf{D}_1) = -\text{Tr} \{ \mathbf{X}^H \boldsymbol{\Xi}_0 \mathbf{X} \} + \frac{\rho_1}{2} \|\mathbf{U} - \mathbf{X} + \mathbf{D}_1\|_F^2,$$

where $\rho_1 > 0$ is a penalty parameter and \mathbf{D}_1 is the dual variable. Under an ADMM framework, we can update $\{\mathbf{X}, \mathbf{U}, \mathbf{D}_1\}$ by taking the following iterative steps.

$$\mathbf{X}^{t+1} := \arg \min_{\mathbf{X}} \mathcal{L}_1(\mathbf{X}, \mathbf{U}^t, \mathbf{D}_1^t), \quad \text{s.t.} (28b), \quad (30a)$$

$$\mathbf{U}^{t+1} := \arg \min_{\mathbf{U}} \mathcal{L}_1(\mathbf{X}^{t+1}, \mathbf{U}, \mathbf{D}_1^t), \quad \text{s.t.} (28c), \quad (30b)$$

$$\mathbf{D}_1^{t+1} := \mathbf{D}_1^t + \mathbf{U}^{t+1} - \mathbf{X}^{t+1}. \quad (30c)$$

where t is the iteration number, $(\cdot)^t$ denote the last point of $(\cdot)^{t+1}$.

B. Solutions to the Subproblems (30a)-(30b)

1) *Optimization of \mathbf{X} :* Given \mathbf{U} and \mathbf{D}_1 , \mathbf{X} can be updated by solving

$$\min_{\mathbf{X}} -\text{Tr} \{ \mathbf{X}^H \boldsymbol{\Xi}_0 \mathbf{X} \} + \frac{\rho_1}{2} \|\mathbf{U} - \mathbf{X} + \mathbf{D}_1\|_F^2, \quad (31a)$$

$$\text{s.t.} \quad \|\mathbf{X}\|_F^2 = P. \quad (31b)$$

By utilizing the Karush-Kuhn-Tucker (KKT) conditions, the closed form solution to \mathbf{X} can be calculated by

$$\mathbf{X}(\mu_1) = (\mathbf{P}_1 + 2\mu_1 \mathbf{I}_{M_t})^{-1} \mathbf{Q}_1, \quad (32)$$

where μ_1 is the Lagrange multiplier, $\mathbf{P}_1 = \rho_1 \mathbf{I}_{M_t} - (\boldsymbol{\Xi}_0 + \boldsymbol{\Xi}_0^H)$ and $\mathbf{Q}_1 = \rho_1 (\mathbf{U} + \mathbf{D}_1)$.

To find the optimal solution μ_1 , we define the eigen-decomposition of \mathbf{P}_1 as $\mathbf{P}_1 = \mathbf{G}_1 \boldsymbol{\Sigma}_1 \mathbf{G}_1^H$. Then, (32) can be rewritten as

$$\mathbf{X}(\mu_1) = \mathbf{G}_1 (\boldsymbol{\Sigma}_1 + 2\mu_1 \mathbf{I}_{M_t})^{-1} \mathbf{G}_1^H \mathbf{Q}_1. \quad (33)$$

Substituting (33) into the constraint (31b), we can obtain

$$\|\mathbf{X}\|_F^2 = \sum_{m=1}^{M_t} \frac{\Psi_1(m,m)}{(\boldsymbol{\Sigma}_1(m,m) + 2\mu_1)^2} = P, \quad (34)$$

where $\Psi_1 = \mathbf{G}_1^H \mathbf{Q}_1 \mathbf{Q}_1^H \mathbf{G}_1$. Based on (34), the optimal solution μ_1^{t+1} can be found using Newton's or bisection method. Finally, the optimal \mathbf{X}^{t+1} can be calculated by substituting the optimal μ_1^{t+1} into (33).

2) *Optimization of \mathbf{U} :* Given \mathbf{X} and \mathbf{D}_1 , \mathbf{U} can be updated by solving

$$\min_{\mathbf{U}} \|\mathbf{U} - \mathbf{X} + \mathbf{D}_1\|_F^2, \quad \text{s.t.} \quad |\mathbf{U}(m,l)|^2 \leq \frac{\kappa P}{M_t L}, \forall m,l. \quad (35)$$

Problem (35) can be decoupled into the following ML consensus problem.

$$\min_{\mathbf{U}(m,l)} |\mathbf{U}(m,l) - \mathbf{X}(m,l) + \mathbf{D}_1(m,l)|^2, \quad (36)$$

$$\text{s.t.} \quad |\mathbf{U}(m,l)|^2 \leq \frac{\kappa P}{M_t L}, \forall m,l,$$

which can be solved by the KKT conditions, and the corresponding Lagrange function is $\mathcal{L}_{1,2}(\mathbf{U}(m,l), \lambda_{m,l}) = |\mathbf{U}(m,l) - \mathbf{X}(m,l) + \mathbf{D}_1(m,l)|^2 - \lambda_{m,l} (\frac{\kappa P}{M_t L} - |\mathbf{U}(m,l)|^2)$, where $\lambda_{m,l}, \forall m,l$ is the Lagrange multiplier.

Then, by taking the first-order optimality condition, we can calculate $\mathbf{U}(m,l)$ by

$$\mathbf{U}(m,l) = \frac{\mathbf{X}(m,l) - \mathbf{D}_1(m,l)}{1 + \lambda_{m,l}}, \quad \forall m,l. \quad (37)$$

There are two cases for the value of $\lambda_{m,l}$ as follows.

- *Case 1:* $\lambda_{m,l} = 0$. Substitute $\lambda_{m,l} = 0$ into (37), if $|\mathbf{U}(m,l)|^2 \leq \frac{\kappa P}{M_t L}$ is satisfied, we obtain $\mathbf{U}(m,l) = \mathbf{X}(m,l) - \mathbf{D}_1(m,l)$.

- *Case 2:* $\lambda_{m,l} > 0$. There must be a relationship

$$\frac{\kappa P}{M_t L} - |\mathbf{U}(m,l)|^2 = 0. \quad (38)$$

By substituting (37) into (38), we can obtain

$$\frac{\kappa P}{M_t L} - \left| \frac{\mathbf{X}(m,l) - \mathbf{D}_1(m,l)}{1 + \lambda_{m,l}} \right|^2 = 0, \quad (39)$$

whose optimal solution is given by

$$\lambda_{m,l}^{t+1} = -1 + \sqrt{\frac{\kappa P}{M_t L} \frac{1}{|\mathbf{X}(m,l) - \mathbf{D}_1(m,l)|}}. \quad (40)$$

The optimal solution to $\mathbf{U}^{t+1}(m,l)$ is obtained by plugging the optimal $\lambda_{m,l}^{t+1}$ into (37).

C. Complexity and Convergence Performance Analysis

Finally, we analyze the complexity of the proposed PCRB oriented waveform design method and present the convergence performance of the proposed algorithm.

1) *Complexity Analysis*: The complexity of the proposed PCRB oriented waveform design includes two parts as follows.

- **Pre-calculation of distribution parameters**: Computing $\Xi_0, \Xi_1, \Xi_2, \Xi_3$ with integration operation need the complexity of $\mathcal{O}(M_t^2 N_{\text{int}})$ and computing Λ needs the complexity of $\mathcal{O}(K^2 N_{\text{int}})$, where $\mathcal{O}(N_{\text{int}})$ represents the complexity of integrating a function.

- **Updating in waveform design algorithm**: Updating \mathbf{X} needs a complexity of $\mathcal{O}(M_t^3)$ and updating \mathbf{U} needs a complexity of $\mathcal{O}(M_t L)$. The complexity of the proposed PCRB oriented algorithm is $\mathcal{O}(N_{\text{ite}}(M_t^3 + M_t L))$, where N_{ite} is the iteration number in the ADMM framework.

To sum up, the total complexity of the proposed PCRB oriented waveform design method is $\mathcal{O}(N_{\text{ite}}(M_t^3 + M_t L) + N_{\text{int}}(K^2 + M_t^2))$.

2) *Convergence Performance*: Convergence of the proposed algorithm is characterized by the following proposition.

Proposition 3: For $\rho_1 > \sqrt{3}\|\Xi_0 + \Xi_0^H\|_F$, the sequence $\{\mathbf{X}^t, \mathbf{U}^t, \mathbf{D}^t\}$ generated by the ADMM-based waveform design algorithm via PCRB oriented method has the following properties

- 1) The augmented Lagrange function \mathcal{L}_1 is decent during $\{\mathbf{X}, \mathbf{U}, \mathbf{D}_1\}$ update;
- 2) The augmented Lagrange function $\mathcal{L}_1(\mathbf{X}, \mathbf{U}, \mathbf{D}_1)$ is lower bounded for all t and converges as $t \rightarrow +\infty$;
- 3) The residual error $\lim_{t \rightarrow \infty} \|\mathbf{U}^t - \mathbf{X}^t\|_F^2 = 0$.

Proof: Please refer to SM Appendix C. ■

V. SOLUTION TO PSBP ORIENTED WAVEFORM DESIGN

In this section, we first transform the fair PSBP waveform design problem (24) into a more tractable form, and derive a corresponding solution. Then, we extend the solution to the integrated PSBP waveform design (25). Finally, a summary of the proposed algorithms for both problems is given.

A. Problem Reformulation of (24)

1) *Step 1: Reformulation of (24)*. Since the problem (24) is a complicated max-min problem, we first equivalently transform it to a more tractable form by introducing an auxiliary variable η as

$$\begin{cases} \min_{\mathbf{X}} & -\eta & (41a) \\ \text{s.t.} & \|\mathbf{X}\|_F^2 = P & (41b) \\ & |\mathbf{X}(m,l)|^2 \leq \frac{\kappa P}{M_t L}, \forall m,l & (41c) \\ & \frac{1}{f(\theta_p)} \|\mathbf{a}_t^H(\theta_p) \mathbf{X}\|_F^2 \geq \eta, \forall \theta_p \in \Theta, & (41d) \end{cases}$$

2) *Step 2: Application of ADMM Framework to $\mathcal{P}_{\text{PSBP},\mathbf{X}}^{2-2}$* . To derive an efficient solution to $\mathcal{P}_{\text{PSBP},\mathbf{X}}^{2-2}$, we propose introducing several auxiliary variables \mathbf{T} and $\{\mathbf{g}_p\}$ to decouple the constraints, leading to the following problem.

$$\mathcal{P}_{\text{PSBP},\mathbf{X}}^{2-3} \begin{cases} \min_{\mathbf{X}, \mathbf{T}, \{\mathbf{g}_p\}} & -\eta & (42a) \\ \text{s.t.} & \|\mathbf{X}\|_F^2 = P & (42b) \\ & |\mathbf{T}(m,l)|^2 \leq \frac{\kappa P}{M_t L}, \forall m,l & (42c) \\ & \frac{1}{f(\theta_p)} \|\mathbf{g}_p\|_F^2 \geq \eta, \forall \theta_p \in \Theta & (42d) \\ & \mathbf{T} = \mathbf{X} & (42e) \\ & \mathbf{g}_p = \mathbf{X}^H \mathbf{a}_t(\theta_p), \forall \theta_p \in \Theta. & (42f) \end{cases}$$

By penalizing the equality constraints (42e) and (42f) into the objective function, the problem (42) can be equivalently rewritten into an AL minimization problem as

$$\mathcal{P}_{\text{PSBP},\mathbf{X}}^{2-4} \begin{cases} \min_{\eta, \mathbf{X}, \mathbf{T}, \{\mathbf{g}_p\}, \mathbf{D}_2, \{\beta_p\}} & \mathcal{L}_2(\eta, \mathbf{X}, \mathbf{T}, \{\mathbf{g}_p\}, \mathbf{D}_2, \{\beta_p\}) & (43a) \\ \text{s.t.} & (42b) - (42d). & (43b) \end{cases}$$

The associated AL function via penalizing the equality constraints (42e) and (42f) is given by

$$\begin{aligned} \mathcal{L}_2(\eta, \mathbf{X}, \mathbf{T}, \{\mathbf{g}_p\}, \mathbf{D}_2, \{\beta_p\}) &= -\eta + \frac{\rho_2}{2} \|\mathbf{T} - \mathbf{X} + \mathbf{D}_2\|_F^2 \\ &+ \frac{\rho_3}{2} \sum_{\theta_p \in \Theta} \|\mathbf{g}_p - \mathbf{X}^H \mathbf{a}_t(\theta_p) + \beta_p\|_F^2, \end{aligned}$$

where $\rho_2, \rho_3 > 0$ are penalty parameters, \mathbf{D}_2 and $\{\beta_p\}$ are dual variables. Similarly, under an ADMM framework, we can update $\{\mathbf{X}, \mathbf{T}, \{\mathbf{g}_p\}\}$ by taking the following iterative steps.

$$\begin{aligned} \mathbf{X}^{t+1} &:= \arg \min_{\mathbf{X}} \mathcal{L}_2(\eta^t, \mathbf{X}, \mathbf{T}^t, \{\mathbf{g}_p^t\}, \mathbf{D}_2^t, \{\beta_p^t\}), \\ &\text{s.t. (42b),} \end{aligned} \quad (44a)$$

$$\begin{aligned} \mathbf{T}^{t+1} &:= \arg \min_{\mathbf{T}} \mathcal{L}_2(\eta^t, \mathbf{X}^{t+1}, \mathbf{T}, \{\mathbf{g}_p^t\}, \mathbf{D}_2^t, \{\beta_p^t\}), \\ &\text{s.t. (42c),} \end{aligned} \quad (44b)$$

$$\begin{aligned} \eta^{t+1}, \{\mathbf{g}_p^{t+1}\} &:= \arg \min_{\eta, \{\mathbf{g}_p\}} \mathcal{L}_2(\eta, \mathbf{X}^{t+1}, \mathbf{T}^{t+1}, \{\mathbf{g}_p\}, \mathbf{D}_2^t, \{\beta_p^t\}), \\ &\text{s.t. (42d),} \end{aligned} \quad (44c)$$

$$\mathbf{D}_2^{t+1} := \mathbf{D}_2^t + \mathbf{T}^{t+1} - \mathbf{X}^{t+1}, \quad (44d)$$

$$\beta_p^{t+1} := \beta_p^t + \mathbf{g}_p^{t+1} - (\mathbf{X}^{t+1})^H \mathbf{a}_t(\theta_p), \theta_p \in \Theta, \quad (44e)$$

Note that the subproblems (44a) and (44b) can be solved similarly to the subproblems (30a) and (30b), respectively. To avoid redundancy, we omit the solutions to the subproblems (44a) and (44b), and only present the solution to the subproblem (44c) as follows.

B. Solutions to the Subproblem (44c)

1) *Optimization of $\eta, \{\mathbf{g}_p\}$* : Given other variables, $\eta, \{\mathbf{g}_p\}$ can be updated by solving

$$\min_{\eta, \{\mathbf{g}_p\}} -\eta + \frac{\rho_3}{2} \sum_{\theta_p \in \Theta} \|\mathbf{g}_p - \mathbf{h}_p\|_F^2, \quad (45a)$$

$$\text{s.t. } \frac{1}{f(\theta_p)} \|\mathbf{g}_p\|_F^2 \geq \eta, \forall \theta_p \in \Theta, \quad (45b)$$

where we define $\mathbf{h}_p = \mathbf{X}^H \mathbf{a}_t(\theta_p) - \beta_p$. To find the optimal solution to $\{\mathbf{g}_p\}, \eta$, we take the following steps:

- Step 1: η is fixed, and $\{\mathbf{g}_p\}$ is updated by

$$\min_{\{\mathbf{g}_p\}} \|\mathbf{g}_p - \mathbf{h}_p\|_F^2 \quad \text{s.t.} \quad \|\mathbf{g}_p\|_F^2 \geq f(\theta_p)\eta, \forall \theta_p \in \Theta, \quad (46)$$

whose solution can be calculated as

$$\mathbf{g}_p = \begin{cases} \mathbf{h}_p, & \|\mathbf{h}_p\|_F^2 \geq f(\theta_p)\eta \\ \frac{\mathbf{h}_p}{\sqrt{f(\theta_p)\eta} \|\mathbf{h}_p\|_F}, & \text{otherwise} \end{cases}. \quad (47)$$

- Step 2: Substituting the updated $\{\mathbf{g}_p\}$, the problem (45) can be converted into

$$\min_{\eta} f(\eta) = -\eta + \frac{\rho_3}{2} \sum_{\theta_p \in \Theta} \varpi_p \left(\sqrt{f(\theta_p)\eta} - \|\mathbf{h}_p\|_F \right)^2,$$

where $\varpi_p = \begin{cases} 0, & \|\mathbf{h}_p\|_F^2 \geq f(\theta_p)\eta \\ 1, & \text{otherwise} \end{cases}$. By taking the first and second order derivatives of $f(\eta)$, we can obtain

$$\frac{\partial f(\eta)}{\partial \eta} = -1 + \frac{\rho_3}{2} \sum_{\theta_p \in \Theta} \sqrt{f(\theta_p)} \varpi_p \left(\sqrt{f(\theta_p)} - \|\mathbf{h}_p\|_F \eta^{-1/2} \right),$$

$$\frac{\partial^2 f(\eta)}{\partial^2 \eta} = \frac{\rho_3}{4} \sum_{\theta_p \in \Theta} \sqrt{f(\theta_p)} \varpi_p \|\mathbf{h}_p\|_F \eta^{-3/2}.$$

Obviously, $\frac{\partial^2 f(\eta)}{\partial^2 \eta} \geq 0$ and then $\frac{\partial f(\eta)}{\partial \eta}$ is monotonically increasing. Applying the first-order optimality condition, we can obtain the optimal η^{t+1} by solving $\frac{\partial f(\eta)}{\partial \eta} = 0$ with Newton's or bisection method.

C. Extension to Solution to the Integrated PSBP Waveform Design Problem (25)

1) *Step 1: Application of ADMM Framework to $\mathcal{P}_{\text{PSBP}, \mathbf{X}}^{3-1}$.* To derive an efficient solution to $\mathcal{P}_{\text{PSBP}, \mathbf{X}}^{3-1}$, we introduce an auxiliary variable \mathbf{V} to decouple the objective and constraints, leading to the following problem.

$$\mathcal{P}_{\text{PSBP}, \mathbf{X}}^{3-2} \begin{cases} \min_{\mathbf{X}, \mathbf{V}} & - \sum_{\theta_p \in \Theta} f(\theta_p) \|\mathbf{a}_t^H(\theta_p) \mathbf{X}\|_F^2 & (48a) \\ \text{s.t.} & \|\mathbf{X}\|_F^2 = P & (48b) \\ & |\mathbf{V}(m, l)|^2 \leq \frac{\kappa P}{M_t L}, \forall m, l & (48c) \\ & \mathbf{X} = \mathbf{V}. & (48d) \end{cases}$$

By penalizing the equality constraint (48d) into the objective function, we convert the problem (48) into an equivalent minimization problem as follows.

$$\mathcal{P}_{\text{PSBP}, \mathbf{X}}^{3-3} \begin{cases} \min_{\mathbf{X}, \mathbf{V}} & \mathcal{L}_3(\mathbf{X}, \mathbf{V}, \mathbf{D}_3) & (49a) \\ \text{s.t.} & (48b) \text{ and } (48c), & (49b) \end{cases}$$

whose associated AL function via penalizing (48d) is

$$\mathcal{L}_3(\mathbf{X}, \mathbf{V}, \mathbf{D}_3) = - \sum_{\theta_p \in \Theta} f(\theta_p) \|\mathbf{a}_t^H(\theta_p) \mathbf{X}\|_F^2 + \frac{\rho_4}{2} \|\mathbf{V} - \mathbf{X} + \mathbf{D}_3\|_F^2,$$

where $\rho_4 > 0$ is the penalty parameter and \mathbf{D}_4 is the dual variable. Under an ADMM framework, $\{\mathbf{X}, \mathbf{V}, \mathbf{D}_3\}$ can be updated by taking the following steps.

$$\mathbf{X}^{t+1} := \arg \min_{\mathbf{X}} \mathcal{L}_3(\mathbf{X}, \mathbf{V}^t, \mathbf{D}_3^t), \quad \text{s.t.} \quad (48b), \quad (50a)$$

$$\mathbf{V}^{t+1} := \arg \min_{\mathbf{V}} \mathcal{L}_3(\mathbf{X}^{t+1}, \mathbf{V}, \mathbf{D}_3^t), \quad \text{s.t.} \quad (48c), \quad (50b)$$

$$\mathbf{D}_3^{t+1} := \mathbf{D}_3^t + \mathbf{V}^{t+1} - \mathbf{X}^{t+1}. \quad (50c)$$

Note that the subproblems (50a) and (50b) can be solved by similar methods of solving (30a) and (30b). To avoid redundancy, we omit the specific derivations.

D. Complexity and Convergence Performance Analysis

Finally, we analyze the complexity of the proposed two PSBP oriented waveform design methods and present the convergence performance of the proposed algorithms.

1) *Complexity Analysis:* Compared with the PCRB oriented waveform design method, the complexity of the PSBP oriented methods only involves the updating in the proposed algorithms as follows.

- **Fair PSBP design algorithm:** Updating \mathbf{X} needs a complexity of $\mathcal{O}(M_t^3)$ and updating \mathbf{T} needs a complexity of $\mathcal{O}(M_t L)$. Solving (45) needs a complexity of $\mathcal{O}(M_t L D)$, where D denotes the sampling number of the angular range. Therefore, the overall complexity of the proposed algorithm is $\mathcal{O}(N_{\text{ite}}(M_t^3 + M_t L D))$, where N_{ite} is the iteration number in the ADMM framework.

- **Integrated PSBP design algorithm:** Updating \mathbf{X} needs a complexity of $\mathcal{O}(M_t^3)$ and updating \mathbf{V} needs a complexity of $\mathcal{O}(M_t L)$. Thus, the overall complexity of the proposed algorithm is $\mathcal{O}(N_{\text{ite}}(M_t^3 + M_t L))$, where N_{ite} is the iteration number in the ADMM framework.

2) *Convergence Performance:* Convergence of the proposed two PSBP oriented waveform design algorithms can be proved similarly to the subsection IV-C2. To avoid redundancy, we omit the specific derivations.

VI. NUMERICAL SIMULATIONS

In this section, we conduct numerical simulations to evaluate the effectiveness of the proposed waveform design algorithms and verify the proposed target location distribution exploitation methods. We start by introducing the simulation setup, followed by three different scenarios corresponding to different distribution models.

A. Simulation Setup

For notation simplification, let PSBP-1 and PSBP-2 denote the specific form of PSBP (23) involved in the fair PSBP design and the integrated PSBP design, respectively. Accordingly, their corresponding waveform design methods are denoted by the PSBP-1 and PSBP-2 oriented waveform methods, respectively.

1) *Parameter Setting:* In the considered colocated radar system, we assume that the colocated radar is equipped with $M_t = M_r = M = 8$ transmit/receive antennas. The number of samples for each radar pulse is $L = 25$ and the sampling number of the angular range $[-\pi/2, \pi/2]$ is $D = 361$. The transmit power is set as $P = 1$, and the radar noise power is set as $\sigma_r^2 = 0$ dB. The complex amplitude is assumed to be $|\zeta|^2 = 0$ dB. All the numerical schemes are analyzed using Matlab 2022b version and performed in a standard PC with Intel(R) CPU(TM) Core i7-10700 2.9 GHz and 16 GB RAM.

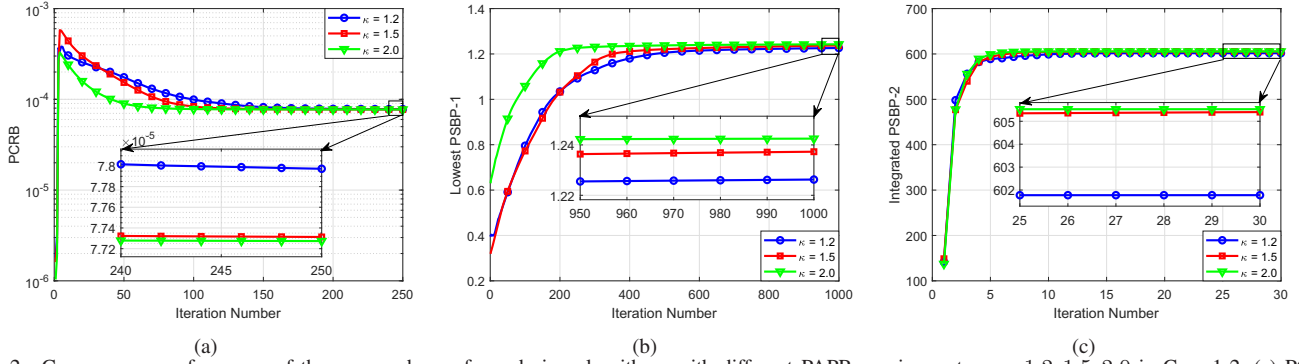


Fig. 2. Convergence performance of the proposed waveform design algorithms with different PAPR requirements $\kappa = 1.2, 1.5, 2.0$ in Case 1-2. (a) PCRB Oriented Method; (b) PSBP-1 Oriented Method; (c) PSBP-2 Oriented Method.

2) *DoA Estimation*: For the DoA estimation based on the waveform optimization methods exploiting target location distribution, we adopt the maximum-a-posteriori (MAP) estimation method, which is given by

$$\hat{\theta}_{\text{MAP}} = \arg \max_{\theta} [\ln(f(\mathbf{Y}|\theta)) + \ln(f(\theta))]. \quad (51)$$

Besides, the MSE between the estimated angle and the actual angle is defined as

$$\text{MSE} = \frac{1}{\mathcal{N}} \sum_{n \in \mathcal{N}} (\hat{\theta}_n - \theta_n)^2, \quad (52)$$

where \mathcal{N} denotes Monte-Carlo trials for each angular point. θ_n and $\hat{\theta}_n$ respectively denote the actual and estimated DoA of the target. In the numerical simulation, we set $\mathcal{N} = 10^4$.

3) *Benchmarks*: To demonstrate the superiority of the proposed algorithms and verify the effectiveness of target location distribution exploitation methods, we include the following benchmarks.

- 1) **CVX-based algorithms**. To demonstrate the superiority of the ADMM-based solutions to $\mathcal{P}_{\text{PCRB}, \mathbf{X}}^{1-1}$, $\mathcal{P}_{\text{PSBP}, \mathbf{X}}^{2-1}$, $\mathcal{P}_{\text{PSBP}, \mathbf{X}}^{3-1}$, we compare the proposed methods with CVX-based algorithms using successive convex approximation (SCA) to simplify and CVX to tackle the resultant problem.
- 2) **CRB oriented Waveform**. In this benchmark, the radar waveform is optimized for an unknown and deterministic angle θ_0 . With other system parameters kept the same, we assume the angular location of the target is $\theta_0 \in \Theta$.
- 3) **Omnidirectional Radar Waveform**. The radiation or reception pattern that is uniform or nearly uniform in all directions is a widely used typical radar waveform.

B. Scenario 1

In this scenario, for the target location distribution, we assume there is $K = 1$ possible angular location interval with the probability $p = 1$. Based on the width of the target occurrence regions, we consider four cases:

Case 1-1: $\Theta = [-\pi/36, \pi/36]$; **Case 1-2**: $\Theta = [-\pi/18, \pi/18]$; **Case 1-3**: $\Theta = [-\pi/9, \pi/9]$; **Case 1-4**: $\Theta = [-\pi/6, \pi/6]$.

1) *Convergence Performance of Algorithm*: In Fig. 2, we present the convergence performance of the proposed waveform design algorithms via PCRB, PSBP-1, and PSBP-2 oriented methods, with different PAPR requirements $\kappa = 1.2, 1.5, 2.0$ for **Case 1-2**. Fig. 2(a), Fig. 2(b) and Fig. 2(c)

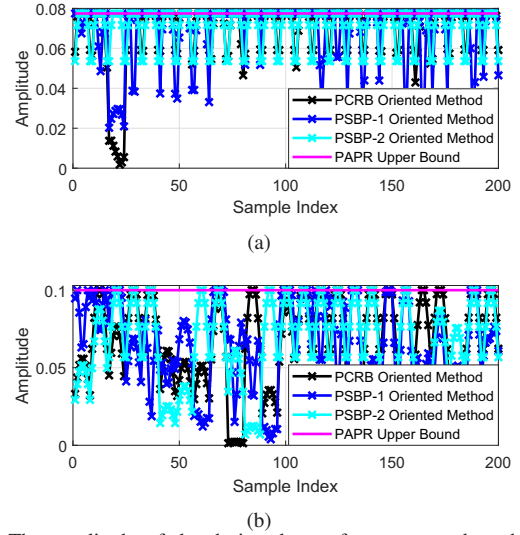


Fig. 3. The amplitude of the designed waveform proposed methods with different PAPR requirements in Case 1-2. (a) PAPR requirement $\kappa = 1.2$. (b) PAPR requirement $\kappa = 2.0$.

plot the PCRB, the lowest PSBP-1 and the integrated PSBP-2 versus the iteration number with different κ , respectively. It can be observed that with the iteration number increasing, the values of PCRB, the lowest PSBP-1, and integrated PSBP-2 reach stationary, which validates the convergence of the proposed algorithms. Moreover, with higher PAPR κ , the PCRB becomes lower, while the lowest PSBP-1 and integrated PSBP-2 become higher. This validates that the higher DoF introduced by the higher PAPR can improve the radar performance.

2) *Amplitude of Designed Waveform with Different PAPR*: In Fig. 3, we show the amplitude of the radar waveform designed by the proposed three methods. The sample index is defined as $l \times m, \forall l = 1, \dots, L, m = 1, \dots, M_t$. Specifically, Figs. 3(a), 3(b) plot the amplitude of the waveform with the PAPR requirement $\kappa = 1.2$ and $\kappa = 2.0$, respectively. It can be seen that the waveform amplitudes obtained by all the proposed methods are not higher than the PAPR upper bound. These results demonstrate the effectiveness of the proposed methods in ensuring that the waveform PAPR complies with hardware specifications in the practical scenario.

3) *Beam pattern Performance*: In Fig. 4, we compare the radar beam pattern obtained by the proposed three methods in different distribution cases. As shown in Fig. 4(a), when the width of the target distribution region is small, the mainlobe levels can be guaranteed to be high on the angular location

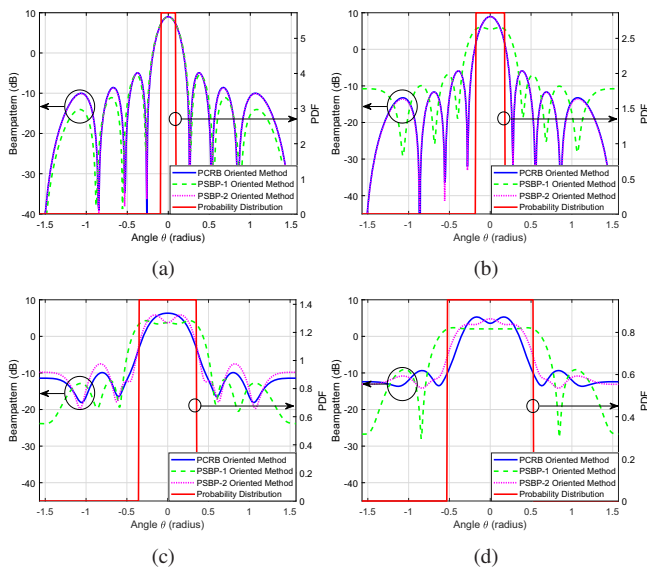


Fig. 4. Comparisons of the radar beampattern obtained by the proposed methods in different target distribution cases. (a) Case 1-1; (b) Case 1-2; (c) Case 1-3; (d) Case 1-4.

region with high target occurrence probability. As the width of the target distribution region becomes larger, we can see that the PSBP-1 oriented method can better maintain a high mainlobe level over the whole target distribution region while the PCRB and PSBP-2 oriented methods can only guarantee a relatively higher level on the narrow central region at a cost of level reduction on the edge of the target distribution region. This shows that the PSBP-1 oriented method can maintain a satisfactorily higher mainlobe level on wide angular regions than the other methods.

4) *DoA Estimation Performance*: In Fig. 5, we compare the DoA estimation performance of the waveform designed by the proposed ADMM-based algorithms and CVX-based algorithms in different target distribution cases by plotting the MSE versus the radar SNR. It can be seen in Fig. 5(a) that the curves of MSEs obtained by all the algorithms are nearly superimposable on the curve of the theoretical PCRB in Case 1-1. As the width of target distribution regions gets larger, the MSE curves get away from the PCRB curves, as shown from Fig. 5(b) to Fig. 5(d). Specifically, in the case of wider target distribution regions, the MSE curves of PSBP-1 oriented method can reach the PCRB bound at a relatively lower SNR, followed by the PSBP-2 oriented method, while the MSE curves of PCRB oriented method approach the PCRB curves at a higher SNR. These results show that in a single-occurrence-region scenario, the DoA estimation performance of the waveform designed by the PSBP-1 oriented algorithm is the best among the proposed three algorithms, followed by the PSBP-2 oriented algorithm, and the PCRB oriented algorithm in the last position. We can also notice that the MSE curves of the proposed ADMM-based algorithms are close to those of the CVX-based algorithms. This validates the effectiveness of the proposed ADMM-based waveform design algorithms.

5) *Computation Time*: Table I presents the computation time of the proposed ADMM-based algorithms and CVX-based algorithms for three waveform design methods in different cases. Generally, it can be seen that the computation

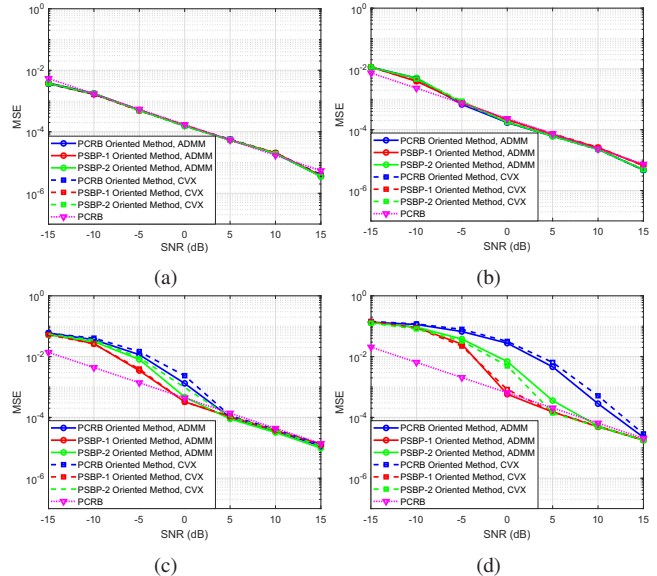


Fig. 5. Comparisons of DoA estimation performance by the proposed ADMM-based algorithms and the CVX-based algorithms in different target distribution cases: the MSE versus SNR. (a) Case 1-1; (b) Case 1-2; (c) Case 1-3; (d) Case 1-4.

time of the proposed ADMM-based algorithms is considerably lower than the CVX-based algorithms. This indicates that the proposed ADMM-based algorithms have great potential to realize real-time computation in practice. Moreover, for the ADMM-based algorithm, we notice that the PSBP-2 oriented algorithm takes nearly 0.1 seconds, the PCRB oriented algorithm takes 1-2 seconds, and the PSBP-1 oriented algorithm takes 10-30 seconds.

TABLE I
COMPUTATION TIME OF THE PROPOSED ADMM-BASED ALGORITHMS AND CVX-BASED ALGORITHMS (UNIT: SECOND)

Method		Case 1-1	Case 1-2	Case 1-3	Case 1-4
PCRB Oriented	ADMM	1.812	1.728	2.103	1.757
	CVX	940.017	1170.235	1459.215	1694.736
PSBP-1 Oriented	ADMM	10.273	14.144	21.754	29.346
	CVX	797.727	845.498	878.421	905.318
PSBP-2 Oriented	ADMM	0.120	0.123	0.145	0.152
	CVX	844.462	881.488	882.686	884.310

Combining Figs. 2-5 and Table I, we provide insights that, although PSBP-1 can achieve better beampattern and DoA estimation, the design time cost of PSBP-1 is relatively higher than the other two methods. This suggests that every target location distribution exploitation method has its pros and cons. Therefore, it is important to choose a more suitable waveform design algorithm when considering the trade-off between computation time requirements and radar performance in practice.

C. Scenario 2

In this scenario, for target location distribution, we assume there are $K = 2$ possible angular location intervals with the probability $p_1 = p_2 = 0.5$. Specifically, based on the separation width of target distribution intervals, we consider six cases:

Case 2-1: $\Theta = [-3\pi/36, -\pi/36] \cup [\pi/36, 3\pi/36]$;

Case 2-2: $\Theta = [-5\pi/36, -3\pi/36] \cup [\pi/36, 3\pi/36]$;

Case 2-3: $\Theta = [-7\pi/36, -5\pi/36] \cup [\pi/36, 3\pi/36]$;

Case 2-4: $\Theta = [-9\pi/36, -7\pi/36] \cup [\pi/36, 3\pi/36]$;

Case 2-5: $\Theta = [-11\pi/36, -9\pi/36] \cup [\pi/36, 3\pi/36]$;

Case 2-6: $\Theta = [-13\pi/36, -11\pi/36] \cup [\pi/36, 3\pi/36]$.

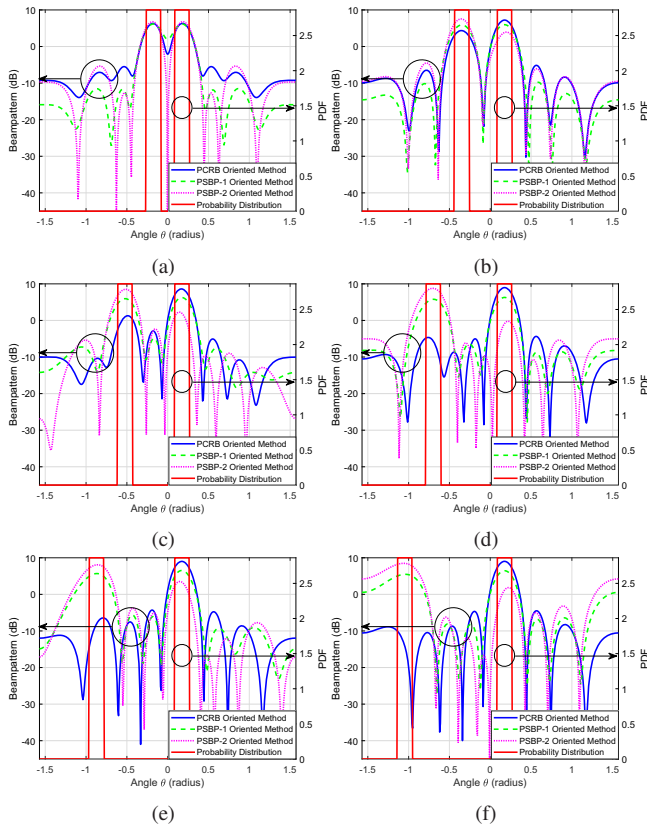


Fig. 6. Comparisons of the radar beampattern obtained by the proposed methods in different target distribution cases. (a) Case 2-1; (b) Case 2-2; (c) Case 2-3; (d) Case 2-4; (e) Case 2-5; (f) Case 2-6.

1) *Beampattern Performance*: Fig. 6 presents the radar beampatterns obtained by the proposed methods from Case 2-1 to Case 2-6. It can be seen that both methods can achieve relatively higher mainlobe levels on the angular regions with high target occurrence probability. Specifically, the PCRb oriented method can realize a higher mainlobe level on the angular interval that is closer to the central angle albeit with a sacrifice in the mainlobe levels on the other angular interval, while the PSBP-2 oriented method has the opposite effect. We can also observe that the mainlobe levels obtained by the PSBP-1 oriented method are guaranteed high on both target distribution intervals. This phenomenon becomes more obvious with the separation width increasing, as presented from Fig. 6(a) to Fig. 6(f). The results show that the PCRb oriented method can improve the mainlobe level on the angular intervals closer to the central angle, the PSBP-2 oriented method can improve the mainlobe level on the angular intervals far away from the central angle, and the PSBP-2 oriented method has a better mainlobe level control on each target distribution interval.

2) *DoA Estimation Performance*: In Fig. 7, we compare the radar DoA estimation performance of the proposed methods in different target distribution cases (from Case 2-1 to Case 2-6) by plotting MSEs versus the separation width. It can be seen that MSEs of DoA estimation increase with separation width increasing and the MSEs become more distant from the PCRb with the increasing separation width, except for the PSBP-2 oriented method at the last two points. We can also observe that the MSE of DoA estimation obtained by the PSBP-1 oriented method is closer to the PCRb, followed by the PSBP-

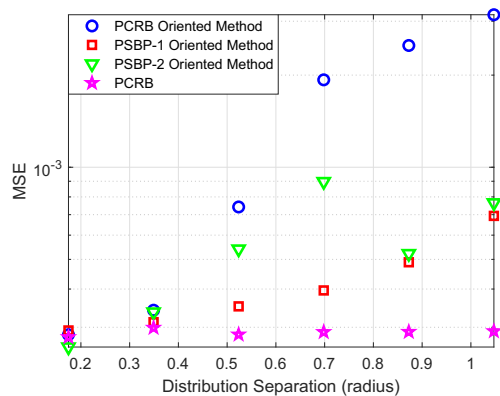


Fig. 7. Comparisons of radar DoA estimation performance in different target distribution cases (From Case 2-1 to Case 2-6): the MSE of the DoA estimation versus the separation width.

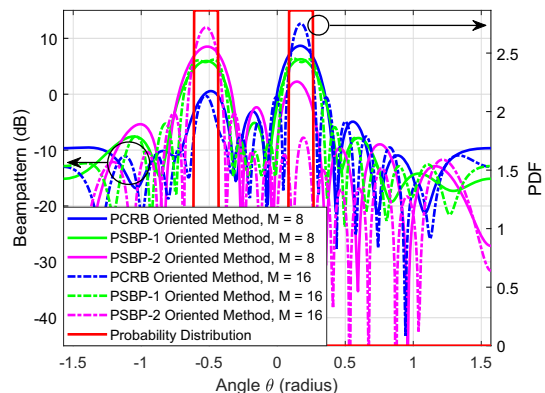


Fig. 8. Beampattern obtained by the proposed methods with a different number of transmit/receive antennas $M = 8, 16$ in Case 2-3.

2 oriented method, and the PCRb oriented method in the last position. Generally speaking, in the multiple-occurrence-region scenario, the results indicate that the DoA estimation performance of the proposed methods degrades when the separation width becomes larger, and the DoA performance of the PSBP-1 oriented method is the best and the PCRb oriented method is the worst.

3) *Impact of Number of Antennas to Beampattern Performance*: In Fig. 8, we present the radar transmit beampattern obtained by the proposed methods, with a different number of transmit/receive antennas $M = 8, 16$, in Case 2-3. We can observe that with the number of antennas increasing, the PCRb oriented method improves the mainlobe level on the angular intervals closer to the central angle while the PSBP-2 oriented method improves the mainlobe level on the angular intervals far away from the central angle, and the PSBP-1 oriented method can better maintain a high mainlobe level among the whole region with high probability. These results indicate that it is necessary to choose a suitable number of transmit/receive antennas to enhance the radar beampattern behavior.

4) *Impact of Number of Antennas to DoA estimation Performance*: In Fig. 9, we present the MSE of the DoA estimation versus the radar SNR for different waveform optimization methods with the number of antennas $M = 8, 16$. It can be seen that the MSEs of DoA estimation obtained by all the methods are decreasing with the radar SNR increasing, and are bounded by the corresponding PCRb/CRb. With the number of antennas increasing, the PCRb/CRb and the MSE obtained

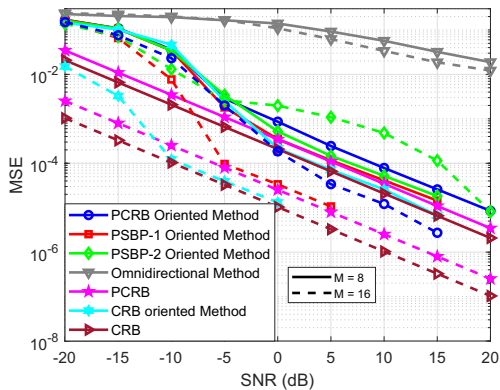


Fig. 9. Comparisons of radar DoA estimation performance with a different number of transmit/receive antennas $M = 8, 16$: the MSE of the DoA estimation versus the radar SNR.

by the PSBP-1 oriented, PCRB oriented and CRB oriented methods becomes lower, while the MSEs obtained by the PSBP-2 oriented methods become higher. Specifically, with $M = 16$, the MSEs obtained by the PSBP-1 oriented method are the closest to the PCRB, followed by the PCRB oriented method, and the PSBP-2 oriented method are the farthest from the PCRB. Besides, the MSEs of DoA estimation obtained by the CRB oriented are always close to the CRB with a high enough SNR. This indicates that a higher number of antennas improves the DoA estimation performance of the PSBP-1, PCRB, and CRB oriented methods but degrades the DoA estimation performance of the PSBP-2 oriented methods. Additionally, the proposed methods can realize significantly lower MSE than the omnidirectional method. This demonstrates that the proposed waveform optimization methods can achieve satisfactory DoA estimation performance by exploiting the target location distribution information.

D. Scenario 3

In this scenario, for target location distribution, we assume there are $K = 4$ possible angular points, i.e., $\theta_1 = -\pi/3$, $\theta_2 = -\pi/6$, $\theta_3 = \pi/9$, $\theta_4 = 5\pi/18$, with probabilities $p_1 = 0.15$, $p_2 = 0.25$, $p_3 = 0.4$, $p_4 = 0.2$.

1) *Beampattern Performance*: In Fig. 10, we compare the radar beampattern obtained by the proposed methods with different standard deviation, $\sigma_\theta = \pi/360, \pi/180, \pi/90, \pi/45$. It can be seen from Fig. 10(a) to Fig. 10(d) that with σ_θ increasing, the beampatterns obtained by the proposed methods do not have obvious change. Specifically, the PCRB oriented and PSBP-2 oriented methods generate almost the same beampattern, whose radiation power is not well proportional to the target occurrence probability at certain angular locations. The PSBP-1 oriented method generates beampattern with better probability-proportional mainlobe levels on angular points $\theta_1 = -\pi/3, \theta_2 = -\pi/6, \theta_3 = \pi/9, \theta_4 = 5\pi/18$. These results show that the PSBP-1 oriented method has a better control of levels for radar beampattern than the other two methods.

2) *DoA Estimation Performance*: Fig. 11 plots the MSEs of DoA estimation versus the SNR. We can see that the MSEs obtained by all the methods are close to the PCRB bound when $\sigma_\theta = \pi/360$. When σ_θ increases, the curves of MSEs obtained

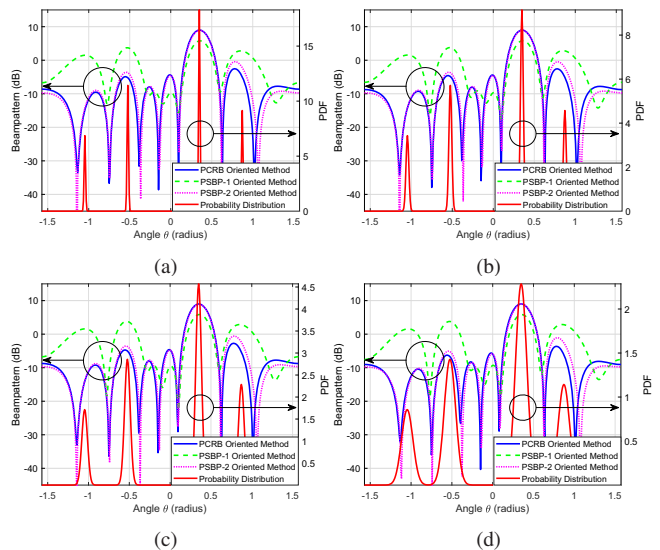


Fig. 10. Comparisons of the radar beampattern obtained by the proposed methods with different standard deviation σ_θ . (a) $\sigma_\theta = \pi/360$; (b) $\sigma_\theta = \pi/180$; (c) $\sigma_\theta = \pi/90$; (d) $\sigma_\theta = \pi/45$.

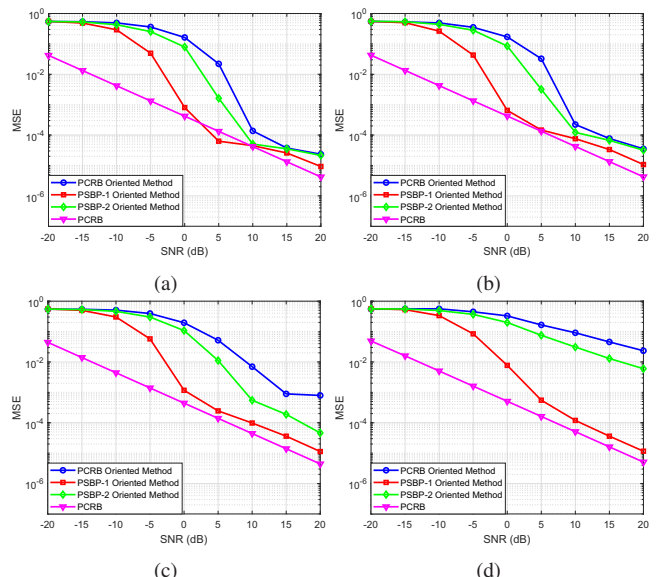


Fig. 11. Comparisons of the DoA estimation performance by the proposed methods with different standard deviation σ_θ . (a) $\sigma_\theta = \pi/360$; (b) $\sigma_\theta = \pi/180$; (c) $\sigma_\theta = \pi/90$; (d) $\sigma_\theta = \pi/45$.

by the PCRB oriented and PSBP-2 oriented methods get far away from the PCRB, while the curves of MSEs obtained by the PSBP-1 oriented method are still close to the PCRB. This indicates that the designed waveform by the proposed PSBP-1 oriented method has better DoA estimation performance than the other two methods.

VII. CONCLUSION

In this paper, we studied and discussed how to exploit target location distribution for MIMO radar waveform design. Specifically, we started by modeling the colocated radar system and the considered target location distribution. With these models at hand, the first category of target location distribution exploitation method, PCRB, was derived from the DoA estimation perspective. With this as a reference, we formulated a PCRB oriented waveform design problem. Then,

a novel PSBP based target location distribution exploitation method was proposed, inspired by the beampattern design perspective. Guided by this, we formulated two PSBP oriented waveform design problems, fair PSBP design, and integrated PSBP design, for different design requirements of desirable radar beampattern. To solve the formulated PCRB and PSBP oriented problems, we devised the corresponding low-complexity and convergency-guaranteed algorithms. Finally, we provided numerical simulations in different scenarios to comprehensively evaluate the radar performance, giving the following insights:

- PCRB serves as the theoretical lower bound of DoA estimation performance; therefore, minimizing PCRB does not always result in satisfactory practical DoA estimation results. However, PCRB has a clear physical meaning, which is important for measuring radar estimation performance.
- The PSBP based target location distribution exploitation can flexibly control the radar beampattern, yielding good DoA estimation performance, especially with PSBP-2. However, the PSBP-2 design is a fairness design problem with the highest computational time complexity.
- Both PCRB and PSBP-based target location distribution exploitation methods are important approaches. In practical radar systems, the choice between PCRB and PSBP should balance computational complexity, optimization time, and DoA estimation performance.

REFERENCES

- [1] E. Fishler *et al.*, "MIMO radar: An idea whose time has come," in *IEEE Radar Conf.* IEEE, 2004, pp. 71–78.
- [2] B. Donnet and I. Longstaff, "MIMO radar, techniques and opportunities," in *Eur. Radar Conf.* IEEE, 2006, pp. 112–115.
- [3] J. Li and P. Stoica, *MIMO radar signal processing*. John Wiley & Sons, 2008.
- [4] —, "MIMO radar with colocated antennas," *IEEE Signal Process. Mag.*, vol. 24, no. 5, pp. 106–114, 2007.
- [5] E. Fishler, A. Haimovich, R. Blum *et al.*, "Performance of MIMO radar systems: Advantages of angular diversity," in *Asilomar Conf. Signals Syst. & Comput.*, vol. 1. IEEE, 2004, pp. 305–309.
- [6] X. Tang, J. Tang, B. Tang, Z. Gao, X. Bi, and J. Du, "A new electronic reconnaissance technology for MIMO radar," in *IEEE CIE Int. Conf. Radar*, vol. 1. IEEE, 2011, pp. 79–83.
- [7] F. Mugnai and D. Tarchi, "Multiple-input multiple-output radar, ground-based mimo sar for ground deformation monitoring," *Eur. J. Rem. Sens.*, vol. 55, no. 1, pp. 604–621, 2022.
- [8] D. Bliss and K. Forsythe, "Mimo radar medical imaging: Self-interference mitigation for breast tumor detection," in *Asilomar Conf. Signals, Syst. & Comput.* IEEE, 2006, pp. 1558–1562.
- [9] Z. Cheng, Z. He, S. Zhang, and J. Li, "Constant modulus waveform design for MIMO radar transmit beampattern," *IEEE Trans. Signal Process.*, vol. 65, no. 18, pp. 4912–4923, 2017.
- [10] W. Fan, J. Liang, and J. Li, "Constant modulus MIMO radar waveform design with minimum peak sidelobe transmit beampattern," *IEEE Trans. Signal Process.*, vol. 66, no. 16, pp. 4207–4222, 2018.
- [11] W. Fan *et al.*, "MIMO radar waveform design for quasi-equiripple transmit beampattern synthesis via weighted l_p -minimization," *IEEE Trans. Signal Process.*, vol. 67, no. 13, pp. 3397–3411, 2019.
- [12] W. Fan, J. Liang *et al.*, "Spectrally-agile waveform design for wideband MIMO radar transmit beampattern synthesis via majorization-ADMM," *IEEE Trans. Signal Process.*, vol. 69, pp. 1563–1578, 2021.
- [13] G. Cui, H. Li, and M. Rangaswamy, "MIMO radar waveform design with constant modulus and similarity constraints," *IEEE Trans. Signal Process.*, vol. 62, no. 2, pp. 343–353, 2013.
- [14] B. Tang and J. Tang, "Joint design of transmit waveforms and receive filters for MIMO radar space-time adaptive processing," *IEEE Trans. Signal Process.*, vol. 64, no. 18, pp. 4707–4722, 2016.
- [15] Z. Cheng, B. Liao, Z. He, Y. Li, and J. Li, "Spectrally compatible waveform design for MIMO radar in the presence of multiple targets," *IEEE Trans. Signal Process.*, vol. 66, no. 13, pp. 3543–3555, 2018.
- [16] X. Yu, K. Alhujaili, G. Cui, and V. Monga, "MIMO radar waveform design in the presence of multiple targets and practical constraints," *IEEE Trans. Signal Process.*, vol. 68, pp. 1974–1989, 2020.
- [17] B. Tang, J. Tang, and Y. Peng, "MIMO radar waveform design in colored noise based on information theory," *IEEE Trans. Signal Process.*, vol. 58, no. 9, pp. 4684–4697, 2010.
- [18] M. M. Naghsh, M. Modarres-Hashemi, M. A. Kerahroodi, and E. H. M. Alian, "An information theoretic approach to robust constrained code design for MIMO radars," *IEEE Trans. Signal Process.*, vol. 65, no. 14, pp. 3647–3661, 2017.
- [19] S. Sen and A. Nehorai, "OFDM MIMO radar with mutual-information waveform design for low-grazing angle tracking," *IEEE Trans. Signal Process.*, vol. 58, no. 6, pp. 3152–3162, 2010.
- [20] I. Bekkerman and J. Tabrikian, "Target detection and localization using MIMO radars and sonars," *IEEE Trans. Signal Process.*, vol. 54, no. 10, pp. 3873–3883, 2006.
- [21] B. Tang, J. Tang, Y. Zhang, and Z. Zheng, "Maximum likelihood estimation of DOD and DOA for bistatic MIMO radar," *Signal Process.*, vol. 93, no. 5, pp. 1349–1357, 2013.
- [22] R. Boyer, "Co-located MIMO radar with orthogonal waveform coding: Cramér-Rao lower bound," in *IEEE Int. Workshop Comp. Adv. in Multi-Sensor Adaptive Process.* IEEE, 2009, pp. 149–152.
- [23] A. Hassani and S. A. Vorobyov, "Transmit energy focusing for DOA estimation in MIMO radar with colocated antennas," *IEEE Trans. Signal Process.*, vol. 59, no. 6, pp. 2669–2682, 2011.
- [24] J. Li, L. Xu, P. Stoica *et al.*, "Range compression and waveform optimization for MIMO radar: A Cramér-Rao bound based study," *IEEE Trans. Signal Process.*, vol. 56, no. 1, pp. 218–232, 2007.
- [25] H. Wang, G. Liao, H. Liu *et al.*, "Joint optimization of MIMO radar waveform and biased estimator with prior information in the presence of clutter," *Eur. J. Adv. Signal Process.*, vol. 2011, pp. 1–13, 2011.
- [26] W. Wu and B. Tang, "Waveform design for higher-resolution localization with MIMO radar," *Signal Process.*, vol. 209, p. 108999, 2023.
- [27] H. van TREES, "Detection, Estimation, and Modulation Theory-Part I," *Detection, Estimation, and Linear Modulation Theory*, pp. 23–46, 1968.
- [28] P. Tichavsky, "Posterior Cramér-Rao bound for adaptive harmonic retrieval," *IEEE Trans. Signal Process.*, vol. 43, no. 5, pp. 1299–1302, 1995.
- [29] P. Tichavsky, C. H. Muravchik, and A. Nehorai, "Posterior Cramér-Rao bounds for discrete-time nonlinear filtering," *IEEE Trans. Signal Process.*, vol. 46, no. 5, pp. 1386–1396, 1998.
- [30] M. Hurtado, T. Zhao, and A. Nehorai, "Adaptive polarized waveform design for target tracking based on sequential Bayesian inference," *IEEE Trans. Signal Process.*, vol. 56, no. 3, pp. 1120–1133, 2008.
- [31] W. Huleihel, J. Tabrikian, and R. Shavit, "Optimal adaptive waveform design for cognitive MIMO radar," *IEEE Trans. Signal Process.*, vol. 61, no. 20, pp. 5075–5089, 2013.
- [32] N. Sharaga and J. Tabrikian, "Optimal adaptive transmit beamforming for cognitive MIMO sonar in a shallow water waveguide," in *Eur. Signal Process. Conf.* IEEE, 2014, pp. 1960–1964.
- [33] N. Sharaga, J. Tabrikian, and H. Messer, "Optimal cognitive beamforming for target tracking in mimo radar/sonar," *IEEE J. Sel. Topics Signal Process.*, vol. 9, no. 8, pp. 1440–1450, 2015.
- [34] H. Godrich, V. M. Chiriach, A. M. Haimovich, and R. S. Blum, "Target tracking in mimo radar systems: Techniques and performance analysis," in *IEEE Radar Conf.*, Jan 2010.
- [35] P. Chavali and A. Nehorai, "Cognitive radar for target tracking in multipath scenarios," in *Int. Waveform Diversity & Design Conf.*, 2010, pp. 000 110–000 114.
- [36] P. Stoica, J. Li, and X. Zhu, "Waveform synthesis for diversity-based transmit beampattern design," *IEEE Trans. Signal Process.*, vol. 56, no. 6, pp. 2593–2598, 2008.
- [37] A. De Maio, Y. Huang, M. Piezzo, S. Zhang, and A. Farina, "Design of optimized radar codes with a peak to average power ratio constraint," *IEEE Trans. Signal Process.*, vol. 59, no. 6, pp. 2683–2697, 2011.
- [38] Z. Cheng, Z. He, B. Liao, and M. Fang, "MIMO radar waveform design with PAPR and similarity constraints," *IEEE Trans. Signal Process.*, vol. 66, no. 4, pp. 968–981, 2017.
- [39] T. W. Anderson *et al.*, *An introduction to multivariate statistical analysis*. Wiley New York, 1958, vol. 2.
- [40] H. L. Van Trees, *Optimum array processing: Part IV of detection, estimation, and modulation theory*. John Wiley & Sons, 2002.

Exploiting Target Location Distribution in MIMO Radar: PCRB vs. PSBP for Waveform Design

Lingyun Xu, *Graduate Student Member, IEEE*, Bowen Wang, *Graduate Student Member, IEEE*,
Huiyong Li and Ziyang Cheng, *Member, IEEE*.

(Supplementary Material)

APPENDIX A PROOF OF PROPOSITION 1

The FIM extracted from the received signal (11a) for estimating $\boldsymbol{\omega}$, is given by [20]

$$\mathbf{F}_S(i, j) = -\mathbb{E} \left\{ \frac{\partial^2 l(\mathbf{Y}|\boldsymbol{\omega})}{\partial \boldsymbol{\omega}(i) \partial \boldsymbol{\omega}(j)} \right\}, \quad i = 1, 2, 3, j = 1, 2, 3 \quad (\text{A-1})$$

We first calculate the partial derivations as

$$\frac{\partial^2 l(\mathbf{Y}|\boldsymbol{\omega})}{\partial \theta^2} = -\frac{2|\varsigma|^2 \text{Tr} \left\{ \mathbf{X}^H \dot{\mathbf{A}}^H(\theta) \dot{\mathbf{A}}(\theta) \mathbf{X} \right\}}{\sigma_r^2} \quad (\text{A-2})$$

$$\frac{\partial^2 l(\mathbf{Y}|\boldsymbol{\omega})}{\partial \theta \partial \varsigma_R} = -\frac{2}{\sigma_r^2} \text{Tr} \left\{ \mathbf{X}^H \dot{\mathbf{A}}^H(\theta) \mathbf{A}(\theta) \mathbf{X} \right\}_{\varsigma_R} \quad (\text{A-3})$$

$$\frac{\partial^2 l(\mathbf{Y}|\boldsymbol{\omega})}{\partial \theta \partial \varsigma_I} = -\frac{2}{\sigma_r^2} \text{Tr} \left\{ \mathbf{X}^H \dot{\mathbf{A}}^H(\theta) \mathbf{A}(\theta) \mathbf{X} \right\}_{\varsigma_I} \quad (\text{A-4})$$

$$\frac{\partial^2 l(\mathbf{Y}|\boldsymbol{\omega})}{\partial [\varsigma_R, \varsigma_I] \partial [\varsigma_R, \varsigma_I]^T} = -\frac{2}{\sigma_r^2} \text{Tr} \left\{ \mathbf{X}^H \mathbf{A}^H(\theta) \mathbf{A}(\theta) \mathbf{X} \right\} \mathbf{I}_2 \quad (\text{A-5})$$

where $\dot{\mathbf{A}}^H(\theta) \dot{\mathbf{A}}(\theta) = \|\dot{\mathbf{a}}_r(\theta)\|_F^2 \mathbf{a}_t(\theta) \mathbf{a}_t^H(\theta) + M_r \dot{\mathbf{a}}_t(\theta) \dot{\mathbf{a}}_t^H(\theta)$, $\dot{\mathbf{A}}^H(\theta) \mathbf{A}(\theta) = M_r \dot{\mathbf{a}}_t(\theta) \mathbf{a}_t^H(\theta)$, $\mathbf{A}^H(\theta) \mathbf{A}(\theta) = M_r \mathbf{a}_t(\theta) \mathbf{a}_t^H(\theta)$ ³. Then, the elements of the FIM \mathbf{F}_S can be expressed as

$$F_{\theta\theta} = \int_{-\pi/2}^{\pi/2} f(\theta) \frac{2|\varsigma|^2 \text{Tr} \left\{ \mathbf{X}^H \dot{\mathbf{A}}^H(\theta) \dot{\mathbf{A}}(\theta) \mathbf{X} \right\}}{\sigma_r^2} d\theta = \frac{2|\varsigma|^2}{\sigma_r^2} \text{Tr} \left\{ \mathbf{X}^H \boldsymbol{\Xi}_1 \mathbf{X} \right\} \quad (\text{A-6})$$

$$\mathbf{F}_{\theta\varsigma}(1, 1) = \int_{-\pi/2}^{\pi/2} f(\theta) \frac{2}{\sigma_r^2} \text{Tr} \left\{ \mathbf{X}^H \dot{\mathbf{A}}^H(\theta) \mathbf{A}(\theta) \mathbf{X} \right\}_{\varsigma_R} d\theta = \frac{2\varsigma_R}{\sigma_r^2} \text{Tr} \left\{ \mathbf{X}^H \boldsymbol{\Xi}_2 \mathbf{X} \right\} \quad (\text{A-7})$$

$$\mathbf{F}_{\theta\varsigma}(1, 2) = \int_{-\pi/2}^{\pi/2} f(\theta) \frac{2}{\sigma_r^2} \text{Tr} \left\{ \mathbf{X}^H \dot{\mathbf{A}}^H(\theta) \mathbf{A}(\theta) \mathbf{X} \right\}_{\varsigma_I} d\theta = \frac{2\varsigma_I}{\sigma_r^2} \text{Tr} \left\{ \mathbf{X}^H \boldsymbol{\Xi}_2 \mathbf{X} \right\} \quad (\text{A-8})$$

$$\mathbf{F}_{\varsigma\varsigma} = \int_{-\pi/2}^{\pi/2} f(\theta) \frac{2}{\sigma_r^2} \text{Tr} \left\{ \mathbf{X}^H \mathbf{A}^H(\theta) \mathbf{A}(\theta) \mathbf{X} \right\} \mathbf{I}_2 d\theta = \frac{2}{\sigma_r^2} \text{Tr} \left\{ \mathbf{X}^H \boldsymbol{\Xi}_3 \mathbf{X} \right\} \mathbf{I}_2 \quad (\text{A-9})$$

³Note that the center of ULA is the phase reference, leading to $\dot{\mathbf{a}}^H(\theta) \mathbf{a}(\theta) = \mathbf{a}^H(\theta) \dot{\mathbf{a}}(\theta) = 0$.

where $\boldsymbol{\Xi}_1 = \int_{-\pi/2}^{\pi/2} f(\theta) (\|\dot{\mathbf{a}}_r(\theta)\|_F^2 \mathbf{a}_t(\theta) \mathbf{a}_t^H(\theta) + M_r \dot{\mathbf{a}}_t(\theta) \dot{\mathbf{a}}_t^H(\theta)) d\theta$, $\boldsymbol{\Xi}_2 = M_r \int_{-\pi/2}^{\pi/2} f(\theta) \dot{\mathbf{a}}_t(\theta) \mathbf{a}_t^H(\theta) d\theta$, $\boldsymbol{\Xi}_3 = M_r \int_{-\pi/2}^{\pi/2} f(\theta) \mathbf{a}_t(\theta) \mathbf{a}_t^H(\theta) d\theta$.

Based on (A-7) and (A-8), we can easily obtain

$$\mathbf{F}_{\theta\varsigma} = \frac{2}{\sigma_r^2} \text{Tr} \left\{ \mathbf{X}^H \boldsymbol{\Xi}_2 \mathbf{X} \right\} [\varsigma_R, \varsigma_I] \quad (\text{A-10})$$

Due to the symmetry of \mathbf{F}_S , the equality relationship $\mathbf{F}_{\theta\varsigma} = \mathbf{F}_{\theta\varsigma}^H$ is held.

The proof is completed.

APPENDIX B PROOF OF PROPOSITION 2

We can expand the equation (21) by substituting the original expression of $\boldsymbol{\Xi}_1$, $\boldsymbol{\Xi}_2$ and $\boldsymbol{\Xi}_3$ in (B-1). Obviously, we can tackle $q(\mathbf{X})$ in (B-1) by reducing fractions to a common denominator, where the common denominator is $\text{De} = \text{Tr} \left\{ \mathbf{X}^H (M_r \int_{-\pi/2}^{\pi/2} f(\theta) \mathbf{a}_t(\theta) \mathbf{a}_t^H(\theta) d\theta) \mathbf{X} \right\} > 0$ and the numerator is given in (B-2). Applying Cauchy-Schwarz inequality, we can obtain $\text{Nu} \geq 0$, and then $q(\mathbf{X}) \geq 0$. Accordingly, the upper bound of the PCRB, $\overline{\text{PCRB}}_\theta(\mathbf{X})$, can be expressed as

$$\text{PCRB}_\theta(\mathbf{X}) < \left[\Lambda + \frac{2|\varsigma|^2}{\sigma_r^2} \text{Tr} \left\{ \mathbf{X}^H \boldsymbol{\Xi}_0 \mathbf{X} \right\} \right]^{-1} \triangleq \overline{\text{PCRB}}_\theta(\mathbf{X}) \quad (\text{B-3})$$

where $\boldsymbol{\Xi}_0 = \int_{-\pi/2}^{\pi/2} f(\theta) \|\dot{\mathbf{a}}_r(\theta)\|_F^2 \mathbf{a}_t(\theta) \mathbf{a}_t^H(\theta) d\theta$.

The proof is completed.

APPENDIX C PROOF OF PROPOSITION 3

Before proving the Proposition 3 From the iterative steps (30a)-(30c), the following optimality condition holds.

$$\begin{aligned} \mathbf{0} &= \nabla_{\mathbf{X}} \mathcal{L}_1(\mathbf{X}^{t+1}, \mathbf{U}^{t+1}, \mathbf{D}_1^t) \\ &= \nabla f(\mathbf{X}^{t+1}) - \rho_1 (\mathbf{U}^{t+1} - \mathbf{X}^{t+1} + \mathbf{D}_1^t) \\ &= \nabla f(\mathbf{X}^{t+1}) - \rho_1 \mathbf{D}_1^{t+1} \end{aligned} \quad (\text{C-1})$$

where $f(\mathbf{X}) = -\text{Tr} \left\{ \mathbf{X}^H \boldsymbol{\Xi}_0 \mathbf{X} \right\}$. Besides, we obtain the inequality relationship

$$\begin{aligned} &\|\nabla f(\mathbf{X}^{t+1}) - \nabla f(\mathbf{X}^t)\|_F \\ &= \left\| -(\boldsymbol{\Xi}_0 + \boldsymbol{\Xi}_0^H) \mathbf{X}^{t+1} + (\boldsymbol{\Xi}_0 + \boldsymbol{\Xi}_0^H) \mathbf{X}^t \right\|_F \\ &\leq \left\| (\boldsymbol{\Xi}_0 + \boldsymbol{\Xi}_0^H) \right\|_F \|\mathbf{X}^t - \mathbf{X}^{t+1}\|_F \end{aligned} \quad (\text{C-2})$$

$$\text{PCRB}_\theta(\mathbf{X}) = \left[\Lambda + \frac{2|\zeta|^2}{\sigma_r^2} \text{Tr} \left\{ \mathbf{X}^H \left(\int_{-\pi/2}^{\pi/2} f(\theta) \|\dot{\mathbf{a}}_r(\theta)\|_F^2 \mathbf{a}_t(\theta) \mathbf{a}_t^H(\theta) d\theta \right) \mathbf{X} \right\} \right. \\ \left. + \frac{2|\zeta|^2}{\sigma_r^2} \left(\text{Tr} \left\{ \mathbf{X}^H \left(M_r \int_{-\pi/2}^{\pi/2} f(\theta) \dot{\mathbf{a}}_t(\theta) \dot{\mathbf{a}}_t^H(\theta) d\theta \right) \mathbf{X} \right\} - \frac{\left| \text{Tr} \left\{ \mathbf{X}^H \left(M_r \int_{-\pi/2}^{\pi/2} f(\theta) \dot{\mathbf{a}}_t(\theta) \mathbf{a}_t^H(\theta) d\theta \right) \mathbf{X} \right\} \right|^2}{\text{Tr} \left\{ \mathbf{X}^H \left(M_r \int_{-\pi/2}^{\pi/2} f(\theta) \mathbf{a}_t(\theta) \mathbf{a}_t^H(\theta) d\theta \right) \mathbf{X} \right\}} \right) \right]^{-1} \quad (\text{B-1})$$

$$\text{Nu} = \int_{-\pi/2}^{\pi/2} f(\theta) \text{Tr} \{ \mathbf{X}^H (\dot{\mathbf{a}}_t(\theta) \dot{\mathbf{a}}_t^H(\theta)) \mathbf{X} \} d\theta \int_{-\pi/2}^{\pi/2} f(\theta) \text{Tr} \{ \mathbf{X}^H (\mathbf{a}_t(\theta) \mathbf{a}_t^H(\theta)) \mathbf{X} \} d\theta - \left| \int_{-\pi/2}^{\pi/2} f(\theta) \text{Tr} \{ \mathbf{X}^H (\dot{\mathbf{a}}_t(\theta) \mathbf{a}_t^H(\theta)) \mathbf{X} \} d\theta \right|^2 \quad (\text{B-2})$$

Based on (C-1), we have

$$\mathbf{D}_1^{t+1} = \frac{1}{\rho_1} \nabla f(\mathbf{X}^{t+1}) \quad (\text{C-3})$$

Substituting (C-3) into (C-2), we can obtain

$$\|\mathbf{D}^{t+1} - \mathbf{D}^t\|_F = \frac{1}{\rho_1} \|\nabla f(\mathbf{X}^{t+1}) - \nabla f(\mathbf{X}^t)\|_F \\ \leq \frac{1}{\rho_1} \|(\Xi_0 + \Xi_0^H)\|_F \|\mathbf{X}^t - \mathbf{X}^{t+1}\|_F \quad (\text{C-4})$$

Proof of (a): The difference of the augmented Lagrangian (30) can be rewritten as

$$\mathcal{L}_1(\mathbf{X}^{t+1}, \mathbf{U}^{t+1}, \mathbf{D}_1^{t+1}) - \mathcal{L}_1(\mathbf{X}^t, \mathbf{U}^t, \mathbf{D}_1^t) \\ = \underbrace{\mathcal{L}_1(\mathbf{X}^t, \mathbf{U}^{t+1}, \mathbf{D}_1^t) - \mathcal{L}_1(\mathbf{X}^t, \mathbf{U}^t, \mathbf{D}_1^t)}_{(1)} \\ + \underbrace{\mathcal{L}_1(\mathbf{X}^{t+1}, \mathbf{U}^{t+1}, \mathbf{D}_1^{t+1}) - \mathcal{L}_1(\mathbf{X}^{t+1}, \mathbf{U}^{t+1}, \mathbf{D}_1^t)}_{(2)} \quad (\text{C-5}) \\ + \underbrace{\mathcal{L}_1(\mathbf{X}^{t+1}, \mathbf{U}^{t+1}, \mathbf{D}_1^t) - \mathcal{L}_1(\mathbf{X}^t, \mathbf{U}^{t+1}, \mathbf{D}_1^t)}_{(3)}$$

Specifically, the first term (1) is bounded by

$$\mathcal{L}_1(\mathbf{X}^{t+1}, \mathbf{U}^{t+1}, \mathbf{D}_1^{t+1}) - \mathcal{L}_1(\mathbf{X}^{t+1}, \mathbf{U}^{t+1}, \mathbf{D}_1^t) \\ = \frac{\rho_1}{2} \left(2 \|\mathbf{D}_1^{t+1} - \mathbf{D}_1^t\|_F^2 + \|\mathbf{D}_1^{t+1}\|_F^2 - \|\mathbf{D}_1^t\|_F^2 \right) \\ \stackrel{(i-a)}{\leq} \frac{\rho_1}{2} \left(2 \|\mathbf{D}_1^{t+1} - \mathbf{D}_1^t\|_F^2 + \|\mathbf{D}_1^{t+1} - \mathbf{D}_1^t\|_F^2 \right) \quad (\text{C-6}) \\ = \frac{3\rho_1}{2} \|\mathbf{D}_1^{t+1} - \mathbf{D}_1^t\|_F^2 \\ \stackrel{(i-b)}{\leq} \frac{3}{2\rho_1} \|(\Xi_0 + \Xi_0^H)\|_F^2 \|\mathbf{X}^{t+1} - \mathbf{X}^t\|_F^2$$

where (i-a) holds due to the triangle inequality, and (i-b) holds due to (C-4).

It is obvious that the second term (2) is bounded by

$$\mathcal{L}_1(\mathbf{X}^t, \mathbf{U}^{t+1}, \mathbf{D}_1^t) - \mathcal{L}_1(\mathbf{X}^t, \mathbf{U}^t, \mathbf{D}_1^t) \leq 0 \quad (\text{C-7})$$

due to the updating of the ADMM algorithm.

The third term is bounded by

$$\mathcal{L}_1(\mathbf{X}^{t+1}, \mathbf{U}^{t+1}, \mathbf{D}_1^t) - \mathcal{L}_1(\mathbf{X}^t, \mathbf{U}^{t+1}, \mathbf{D}_1^t) \\ = f(\mathbf{X}^{t+1}) - f(\mathbf{X}^t) + \frac{\rho_1}{2} \|\mathbf{U}^{t+1} + \mathbf{D}_1^t - \mathbf{X}^{t+1}\|_F^2 \\ - \frac{\rho_1}{2} \|\mathbf{U}^{t+1} + \mathbf{D}_1^t - \mathbf{X}^t\|_F^2 \\ \stackrel{(ii-a)}{=} f(\mathbf{X}^{t+1}) - f(\mathbf{X}^t) - \frac{\rho_1}{2} \left(\|\mathbf{X}^{t+1} - \mathbf{X}^t\|_F^2 \right. \\ \left. + 2\Re \left\{ \text{Tr} \left\{ (\mathbf{U}^{t+1} - \mathbf{X}^{t+1} + \mathbf{D}_1^t)^H (\mathbf{X}_1^t - \mathbf{X}_1^{t+1}) \right\} \right\} \right) \\ = f(\mathbf{X}^{t+1}) - f(\mathbf{X}^t) - \frac{\rho_1}{2} \|\mathbf{X}^{t+1} - \mathbf{X}^t\|_F^2 \\ - \rho_1 \Re \left\{ \text{Tr} \left\{ (\mathbf{U}^{t+1} - \mathbf{X}^{t+1} + \mathbf{D}_1^t)^H (\mathbf{X}_1^{t+1} - \mathbf{X}_1^t) \right\} \right\} \\ = f(\mathbf{X}^{t+1}) - f(\mathbf{X}^t) - \frac{\rho_1}{2} \|\mathbf{X}^{t+1} - \mathbf{X}^t\|_F^2 \\ - \rho_1 \Re \left\{ \text{Tr} \left\{ (\mathbf{D}_1^{t+1})^H (\mathbf{X}_1^{t+1} - \mathbf{X}_1^t) \right\} \right\} \\ \stackrel{(ii-b)}{=} -\frac{\rho_1}{2} \|\mathbf{X}^{t+1} - \mathbf{X}^t\|_F^2 - (f(\mathbf{X}^t) - f(\mathbf{X}^{t+1})) \\ + \Re \left\{ \text{Tr} \left\{ (\nabla f(\mathbf{X}^{t+1}))^H (\mathbf{X}_1^t - \mathbf{X}_1^{t+1}) \right\} \right\} \\ \stackrel{(ii-c)}{\leq} -\frac{\rho_1}{2} \|\mathbf{X}^{t+1} - \mathbf{X}^t\|_F^2 \quad (\text{C-8})$$

where (ii-a) holds due to the cosine inequality, (ii-b) holds due to (C-3), and (ii-c) holds due to the property of concave function $f(\mathbf{X})$.

Applying (C-6)-(C-8) into (C-5), we can obtain

$$\mathcal{L}_1(\mathbf{X}^{t+1}, \mathbf{U}^{t+1}, \mathbf{D}_1^{t+1}) - \mathcal{L}_1(\mathbf{X}^t, \mathbf{U}^t, \mathbf{D}_1^t) \\ \leq \left(\frac{3}{2\rho_1} \|(\Xi_0 + \Xi_0^H)\|_F^2 - \frac{\rho_1}{2} \right) \|\mathbf{X}^{t+1} - \mathbf{X}^t\|_F^2 \quad (\text{C-9})$$

which means that the value of the augmented Lagrangian (30) is always decreasing during the iterative process when the penalty parameter $\rho_1 > \sqrt{3} \|\Xi_0 + \Xi_0^H\|_F$.

Proof of (b): Based on (29), \mathbf{X}^{t+1} is bounded by the power constraint $\|\mathbf{X}^{t+1}\|_F^2 = P$, and $f(\mathbf{X}^{t+1})$ is continuous, so $f(\mathbf{X}^{t+1})$ is bounded on $[f_{\min}, f_{\max}]$, where f_{\min} is the lower bound of $f(\mathbf{X}^{t+1})$ and f_{\max} is the upper bound of $f(\mathbf{X}^{t+1})$. Since $\|\mathbf{U}^{t+1} - \mathbf{X}^{t+1} + \mathbf{D}_1^{t+1}\|_F^2 \geq 0$, we have $\mathcal{L}_1(\mathbf{X}^{t+1}, \mathbf{U}^{t+1}, \mathbf{D}_1^{t+1}) \geq f_{\min}$. Therefore, the augmented Lagrange function $\mathcal{L}_1(\mathbf{X}^{t+1}, \mathbf{U}^{t+1}, \mathbf{D}_1^{t+1})$ is lower bounded for all t and converges as $t \rightarrow +\infty$ based on (a).

Proof of (c): Based on (a) and (b), setting $\rho_1 > \sqrt{3}\|\Xi_0 + \Xi_0^H\|_F$, we have

$$\lim_{t \rightarrow \infty} \|\mathbf{X}^{t+1} - \mathbf{X}^t\|_F^2 = 0 \quad (\text{C-10})$$

Applying (C-4), we have

$$\lim_{t \rightarrow \infty} \|\mathbf{D}^{t+1} - \mathbf{D}^t\|_F^2 = 0 \quad (\text{C-11})$$

Substituting (30c) into (C-11), we can obtain

$$\lim_{t \rightarrow \infty} \|\mathbf{U}^{t+1} - \mathbf{X}^{t+1}\|_F^2 = 0 \quad (\text{C-12})$$

which proves (c).

The proof is completed.